MIT Open Access Articles

Efficiency of compaction and compositional convection during mafic crystal mush solidification: the Sept Iles layered intrusion, Canada

ORIGINAL PAPER

Efficiency of compaction and compositional convection during mafic crystal mush solidification: the Sept Iles layered intrusion, Canada

Olivier Namur · Bernard Charlier

Abstract Adcumulate formation in mafic layered intrusions is attributed either to gravity-driven compaction, which expels the intercumulus melt out of the crystal matrix, or to compositional convection, which maintains the intercumulus liquid at a constant composition through liquid exchange with the main magma body. These processes are length-scale and time-scale dependent, and application of experimentally derived theoretical formulations to magma chambers is not straightforward. New data from the Sept Iles layered intrusion are presented and constrain the relative efficiency of these processes during solidification of the mafic crystal mush. Troctolites with meso- to ortho-cumulate texture are stratigraphically followed by Fe–Ti oxide-bearing gabbros with adcumulate texture. Calculations of intercumulus liquid fractions based on whole-rock P, Zr, V and Cr contents and detailed plagioclase compositional profiles show that both compaction and compositional convection operate, but their efficiency changes with liquid differentiation. Before saturation of Fe–Ti oxides in the intercumulus liquid, convection is not active due to the stable liquid density distribution within the crystal mush. At this stage, compaction and minor intercumulus liquid crystallization reduce the porosity to 30%. The velocity of liquid expulsion is then too slow compared with the rate of crystal accumulation. Compositional convection starts at Fe–Ti oxide-saturation in the pore melt due to its decreasing density. This process occurs together with crystallization of the intercumulus melt until the residual porosity is less than 10%. Compositional convection is evidenced by external plagioclase rims buffered at An_{61} owing to continuous exchange between the intercumulus melt and the main liquid body. The change from a channel flow regime that dominates in troctolites to a porous flow regime in gabbros results from the increasing efficiency of compaction with differentiation due to higher density contrast between the cumulus crystal matrix and the equilibrium melts and to the bottom-up decreasing rate of crystal accumulation in the magma chamber.

Keywords Magma chamber · Liquid migration · Intercumulus liquid · Plagioclase zoning · Skaergaard · Mushy layer

O. Namur
Département de Géologie, Université de Liège,
Liège 4000, Belgium

O. Namur (✉)
Department of Earth Sciences, University of Cambridge,
Cambridge CB2 3EQ, UK
e-mail: obn21@cam.ac.uk

B. Charlier
Department of Earth, Atmospheric, and Planetary Sciences,
Massachusetts Institute of Technology, Cambridge,
MA 02139-4307, USA

Introduction

Crystal mush compaction due to imbalance between lithostatic and hydrostatic pressure gradients (e.g., McKenzie 1984; Philpotts et al. 1996, 1999; Meurer and Boudreau 1998a; Tegner et al. 2009), and compositional convection resulting in continuous fluid flow exchange between intercumulus melt and overlying liquid (e.g., Huppert and Sparks 1984; Tait et al. 1984; Kerr and Tait

1985, 1986; Morse 1986; Martin et al. 1987; Tait and Jaupart 1989, 1992) are recognized as the main mechanisms of intercumulus melt migration during solidification of mafic crystal mushes. Formation of adcumulates, which have trapped liquid fraction below 7% (Irvine 1982), requires these mechanisms to be highly efficient in segregating the melt from the crystal framework, thought to contain 40–70% intercumulus melt (e.g., Shirley 1986; Philpotts and Carroll 1996; Philpotts et al. 1998; Jerram et al. 1996, 2003; Donev et al. 2004).

Adcumulates are commonly observed in layered intrusions (e.g., Wager and Brown 1968; Campbell 1978; Charlier et al. 2005; Tegner et al. 2009). In the Skaergaard intrusion, their formation has been controversially attributed either to a process of compositional convection (Toplis et al. 2008) or to compaction of the crystal mush (Tegner et al. 2009; McKenzie 2011). The efficiency of compaction is linked to the density contrast between the crystal network and the intercumulus liquid, while that of compositional convection depends on the density difference between the intercumulus liquid and the main magma body. Deciphering the relative role of the two mechanisms requires a detailed knowledge of the crystallization products and of the evolution of residual liquids, a highly debated subject for Skaergaard (Wager and Brown 1968; Hunter and Sparks 1987; Toplis and Carroll 1996; Tegner 1997; Thy et al. 2006, 2009).

The Sept Iles layered intrusion, Canada, exposes a 4.5-km-thick sequence of troctolitic meso- to ortho-cumulates followed by gabbroic accumulates. The cumulate sequence and equilibrium liquid line of descent have been studied in detail (Namur et al. 2010, 2011a). This intrusion is thus appropriate to further document the processes responsible for intercumulus liquid flow in partly molten crystal mush and for the formation of accumulate rocks in cumulate sequences resulting from the crystallization of basalts. In this study, the petrography and geochemistry of cumulates from megacyclic unit 1 (MCU I) of the Sept Iles Layered Series are presented and used to calculate the residual porosity, commonly referred to as the intercumulus liquid fraction. Theoretical models for compaction (McKenzie 1984; Sparks et al. 1985) and compositional convection (Tait et al. 1984; Morse 1986) are presented to constrain the relative efficiency of these two processes. However, given the poor knowledge of some physical properties of mafic crystal mushes (e.g., thickness, viscosity), theoretical models are found to be unable to unambiguously discriminate these processes. Calculated fractions of intercumulus liquid are then used, together with detailed plagioclase compositional profiles, to show that: (1) the solidification of troctolites is characterized by an initial stage where compaction occurs until a porosity of ca. 30%. Further intercumulus liquid migration results from compositional convection that begins after the saturation of Fe–Ti oxides in the intercumulus melt and is efficient until the residual porosity becomes lower than ca. 10%; (2) gabbroic adcumulate rocks probably result from a combination of compositional convection and compaction, both processes being able to start as soon as the cumulus Fe–Ti oxide-bearing crystal framework forms.

The Sept Iles Layered Series MCU I

The Sept Iles layered intrusion is located in Quebec, Canada. It is a large magmatic body of 20,000 km^3 (Loncarevic et al. 1990), dated at 564 ± 4 Ma (U–Pb on zircon; Higgins and van Breemen 1998). The geology of the intrusion was described in detail by Higgins (2005) and Namur et al. (2010, 2011a) who demonstrated that it is made up from base to top of a Layered Series with three megacyclic units (MCU) dominated by troctolite and gabbro, an Upper Border Series comprised of anorthosite, and a mostly granitic Upper Series. The parent magma is an iron-rich tholeiitic basalt (i.e., ferrobasalt), and the sequence of crystallization in the three MCU of the Layered Series is plagioclase + olivine, followed by Fe–Ti oxides (magnetite and ilmenite), then clinopyroxene and finally apatite. In this study, we investigate the first megacyclic unit (MCU I) of the Layered Series because this unit is the most suitable to understand postcumulus processes for two reasons: (1) A complete and continuous section across MCU I is available and (2) the geochemical evolution of this unit corresponds to the differentiation of a single magma batch.

The Layered Series MCU I is 1,785 m thick and is made up from base to top of troctolite (po-C; classification following Irvine 1982; Fig. 1a–c), Fe–Ti oxide-bearing troctolite (pomi-C; Fig. 1d), olivine-bearing gabbro (pomic-C), gabbro (pmic-C; Fig. 1e) and apatite-bearing gabbro (pomica-C; Fig. 1f). The temporary disappearance of olivine in the gabbroic unit (pmic-C) is a well-known feature of cumulate rocks crystallized from tholeiitic liquids (Morse 1990) and has been extensively discussed in Namur et al. (2010, 2011b). Troctolites (po-C) are dominated by plagioclase (54–83 vol.%) and olivine (15–43 vol.%), with intercumulus Fe–Ti oxides (0–4 vol.%), clinopyroxene (0–6 vol.%) and apatite (<1 vol.%; Fig. 2). Very rare small crystals of accessory phases such as zircon and epidote have been observed in the interstices between cumulus phases. Zoning patterns are observed in most plagioclase crystals and are generally represented by a central anorthite-rich core surrounded by a variably thick rim enriched in the albite component (Fig. 1a). Olivine is represented by large (up to 20 mm) subhedral or slightly poikilitic crystals (Fig. 1b). Intercumulus Fe–Ti oxides
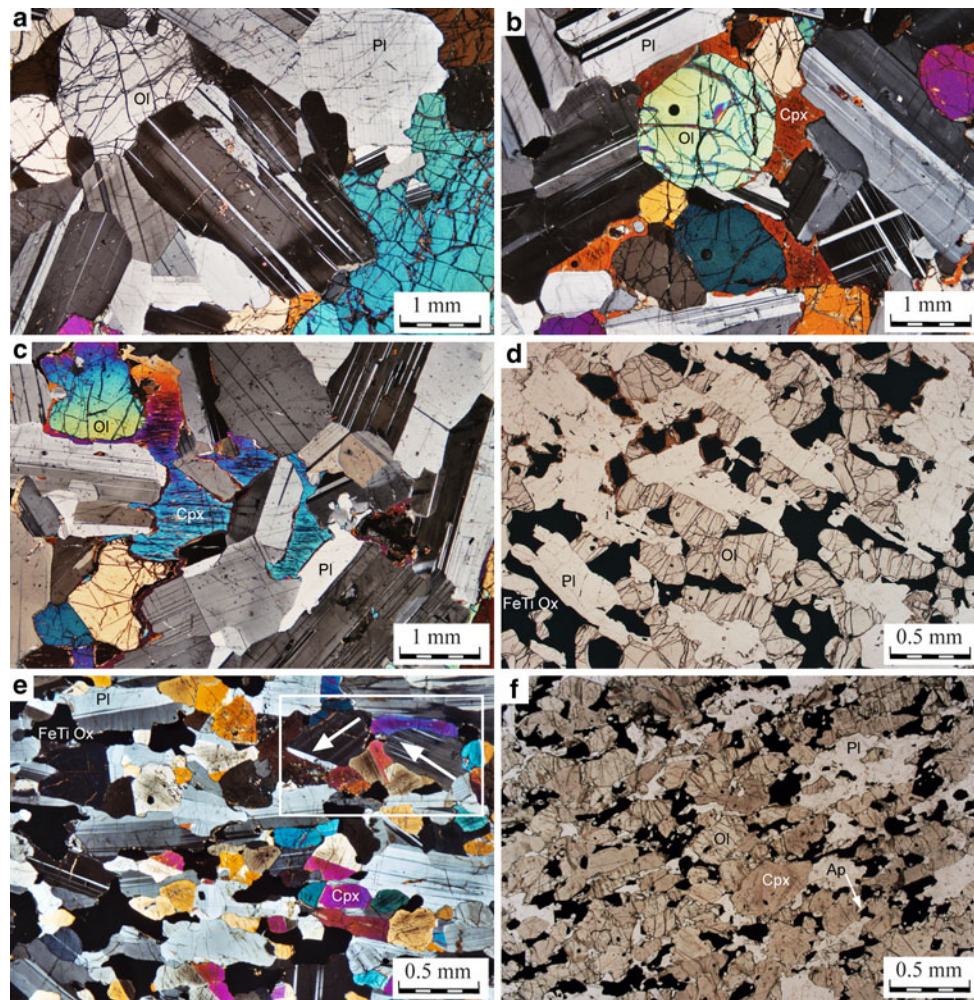
Fig. 1 Photomicrographs of mineral textures and intercumulus assemblages observed in rocks from the Sept Iles Layered Series MCU I. **a** Troctolite (po-C) with lath-shaped plagioclase grains and large subhedral to slightly poikilitic olivine grains. Note the strong zoning in plagioclase grains. Sample DC-9-2451, cross-polarized transmitted light. **b** Troctolite (po-C) with olivine grains surrounded by a rim of intercumulus clinopyroxene. *Black spots* in olivine represent pits of LA-ICP-MS analyses. Sample DC-9-2202, cross-polarized transmitted light. **c** Troctolite (po-C) showing plagioclase and olivine cumulus grains enclosed in a mm-scale clinopyroxene oikocryst. Sample DC-9-2334.5, cross-polarized transmitted light. **d** Fe–Ti oxide-bearing troctolite (pomi-C). Note the mineral lamination described by plagioclase and olivine grains. Sample DC-9-1635, transmitted light. **e** Gabbro (pmic-C). *Arrows* show plagioclase lamination wrapping clinopyroxene grains. Sample DC-91261.5, cross-polarized transmitted light. **f** Apatite-bearing gabbro (pomica-C). DC-9-491.5, transmitted light

occur as small (<1 mm) anhedral patches of ilmenite with minor magnetite, while intercumulus clinopyroxene has crystallized as mm- to cm-scale poikilitic grains or as 50–500 μm coronitic rims surrounding plagioclase and olivine (Fig. 1b, c). Similar rims have recently been interpreted as representing original films of intercumulus melt (Holness 2005; Holness et al. 2007a, b). Intercumulus apatite is observed as very rare 50-μm-long needle-shaped crystals located in the rims of silicate phases or in the interstices between them. From a textural point of view, the troctolites are massive rocks with randomly oriented plagioclase and olivine. Plagioclase is tabular in shape and has relatively low aspect ratio values (length/width of the crystals; average 2:1; Fig. 3a), while olivine is generally

represented by subcircular crystals. Plagioclase triple junctions are consistently 120°, suggesting a good approach to textural equilibrium (Hunter 1987). No evidence for mineral lamination is observed in these rocks (Fig. 1a–c).

Fe–Ti oxide-bearing troctolites (pomi-C) and gabbros (pomic-C, pmic-C and pomica-C) are dominated by plagioclase (3–82 vol.%), Fe–Ti oxides (4–32 vol.%), ±clinopyroxene (2–37 vol.%), ±olivine (2–37 vol.%) and ±apatite (0–8 vol.%; Fig. 2). Plagioclase has crystallized as strongly tabular subhedral to euhedral optically unzoned crystals (0.1–5 mm; Fig. 1d, e). Olivine is represented by small (0.2–4 mm) equant to slightly prismatic euhedral crystals (Fig. 1d). In the pmic-C unit, primary cumulus
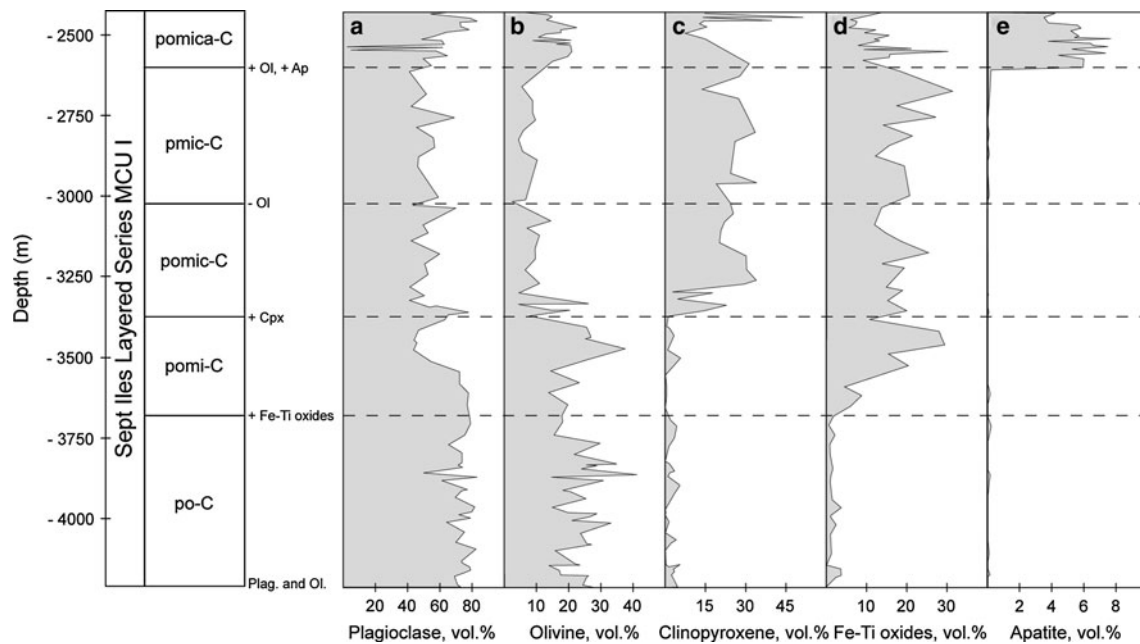
Fig. 2 Sequence of crystallization and mineral modes (vol.%) in the Sept Iles Layered Series MCU I. *a* Plagioclase, *b* olivine, *c* clinopyroxene, *d* Fe–Ti oxides and *e* apatite. Cumulus assemblages follow the nomenclature of Irvine (1982). Mineral abbreviations in cumulus assemblages: p = plagioclase; o = olivine; m = magnetite; i = ilmenite; c = clinopyroxene; a = apatite. Mineral modes have been determined by point-counting on polished thin sections (>1,000 points per sample; see Namur et al. 2010 for details)

olivine is absent and this mineral is only represented by 100- to 500-μm-thick rims around Fe–Ti oxide minerals and clinopyroxene. Clinopyroxene occurs as small (up to 5 mm) subhedral to euhedral prismatic crystals (Fig. 1e). Fe–Ti oxides (6–40 wt%) form large anhedral grains (up to 1 cm; Fig. 1d). Intercumulus apatite occurs as very small needles, while cumulus apatite (pomica-C unit) is found as abundant mm-sized euhedral crystals (Fig. 1f). Fe–Ti oxide-bearing troctolites and gabbros (pomi-C; pomi-C; pmic-C; pomica-C) show a drastic textural change compared with troctolites (po-C). Plagioclase forms long tabular crystals with high aspect ratio values (average 3:1; Fig. 3b), and together with clinopyroxene and locally olivine, they display a very well-defined mineral lamination (Fig. 1d–f). Where primarily defined by plagioclase crystals, the lamination locally wraps small rounded clinopyroxene grains or Fe–Ti oxide patches (Fig. 1e). Plagioclase also locally shows evidence for bent twinning (Fig. 1e), a feature traditionally interpreted as resulting from mineral deformation due to uniaxial stress (Higgins 1991; Meurer and Boudreau 1998b).

Sampling

Seventy-three samples were collected in the Layered Series MCU I. All the samples (ca. 40 cm long) come from drill-core BH84699. Stratigraphic positions of the samples were

corrected for the local dip of the igneous layering, estimated at 30° south and are reported relative to the "0-meter" reference level chosen as the lowest sample containing apatite in MCU II (Namur et al. 2010).

Whole-rock major and trace element compositions were measured by XRF at the University of Liège (Belgium). Mineral compositions were measured by EPMA at the University of Clermont-Ferrand (France) for major elements and by LA-ICP-MS at the Australian National University (Australia) for trace elements. Bulk-rock densities were determined in two ways: using Archimedes principle and by calculation using mineral proportions and mineral compositions. Details of analytical methods, including all the preparation techniques and instrument protocols, are described in Electronic Supplementary Materials.

Results

Mineral compositions

Major elements in plagioclase

Plagioclase core-rim compositional profiles have been measured on crystals oriented perpendicular to {010} for 24 samples of the Layered Series MCU I. In samples from the po-C unit and the lower part of the pomi-C unit, profiles
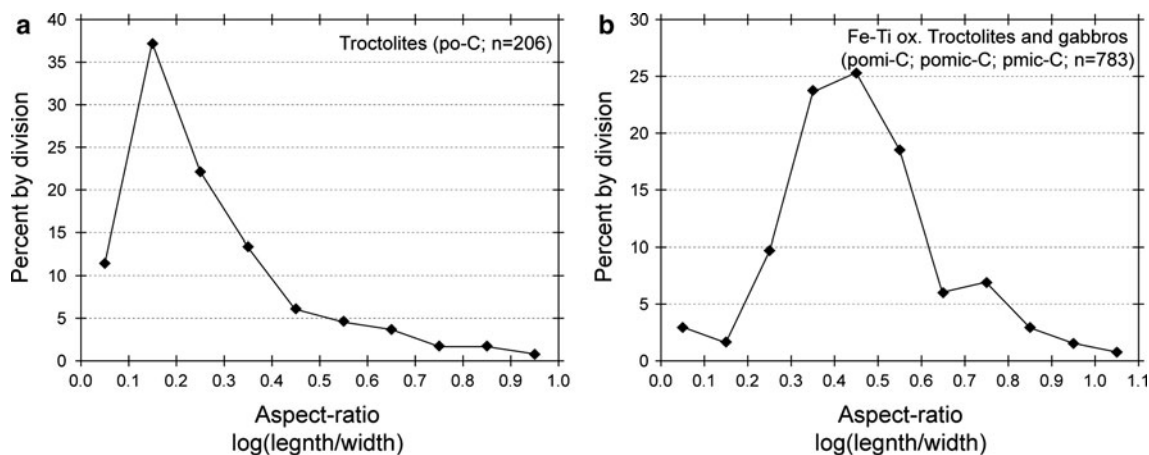
Fig. 3 Distribution of length/width ratios of plagioclase grains. The percentage of crystals that fall within each length/width division is plotted on the vertical axis. a Troctolites (po-C; 206 measurements in 5 samples). b Fe–Ti oxide-troctolites and gabbros (pomi-C; pomic-C; pmic-C; 783 measurements in 10 samples)

toward plagioclase-plagioclase contacts are always zoned and generally show three sections (Fig. 4a–d): a central plateau of relatively constant composition (compositional variations lower than 3 mol% An, with An being [Ca/(Ca + Na)]), a thin zone of decreasing An content and a variably thick external zone with a constant composition of An$_{61\pm1}$, independently of the stratigraphic height of the sample. This external zone is locally extended by a fourth zone with compositions decreasing to significantly lower An contents (Fig. 4c). Compositional profiles toward other cumulus phases (olivine, magnetite or ilmenite) generally show zoning patterns similar to plagioclase-plagioclase contacts, but in rare cases, the central plateau is in direct contact with the other cumulus phase and no significant zoning is observed (Fig. 4d). In samples from the upper part of the pomi-C unit to the top of MCU I, plagioclase profiles do not show any significant zoning and compositional variations are lower than 3 mol% An (Fig. 4e, f).

Compositional characteristics observed at the scale of plagioclase crystals may also be described at a sample scale by plotting all the core and rim data for each sample in histograms (Fig. 5). Core compositions show a relatively symmetric distribution around a well-defined maximum in the mode (Table A1; Supplementary Materials). The compositional variability of plagioclase cores is much more pronounced in the lower part of the MCU I (po-C) than in the upper part (pomi-C to pomica-C). Rim compositions also show a broadly symmetric distribution around a maximum in the mode, while some samples show numerous outliers with lower An content. The range of rim compositions is the largest in samples from the po-C unit and the lower part of the pomi-C unit. Moreover, the mode of rim compositions in this stratigraphic interval has a constant value of 61 ± 1 mol% An, independently of the stratigraphic position of the sample. This value is

significantly lower than the mode of core compositions. Consequently, rim and core compositions as a function of the stratigraphic height are fitted with two different linear regressions that converge at 61 mol% An in the middle part of the pomi-C unit (Fig. 6). In contrast, for samples from the pomic-C unit to the top of MCU I, the mode of rim compositions is almost identical to that of core compositions (Figs. 5, 6).

Trace elements in cumulus phases

Some trace elements have been analyzed in the cumulus phases (P in plagioclase, olivine, clinopyroxene and Fe–Ti oxides; Zr, Cr and V in plagioclase, olivine and Fe–Ti oxides; Table A2; Supplementary Materials) and will be used in the following to determine the contribution of these minerals to the geochemical signature of whole-rock cumulates. This is of crucial importance to accurately calculate the intercumulus liquid fractions in these rocks.

In plagioclase and olivine, P ranges, respectively, from 54 to 129 ppm and from 82 to 295 ppm and increases continuously from the po-C unit to the top of the pmic-C unit, before decreasing in the pomica-C unit, probably as a result of P-depletion in the liquid due to cumulus apatite crystallization. The P content of clinopyroxene does not show any systematic evolution with differentiation and scatters between 43 and 75 ppm, while P concentrations are lower than 2 ppm in magnetite and 3 ppm in ilmenite. The Zr content is below the detection limit (<0.1 ppm) in olivine and plagioclase. Cr and V contents in plagioclase are very low (<2 ppm) and do not show any systematic evolution with differentiation. Cr in olivine scatters between 3 and 5 ppm in the po-C unit and then decreases to values lower than 1 ppm toward the top of the Layered Series MCU I. V in olivine is very low (<2 ppm)
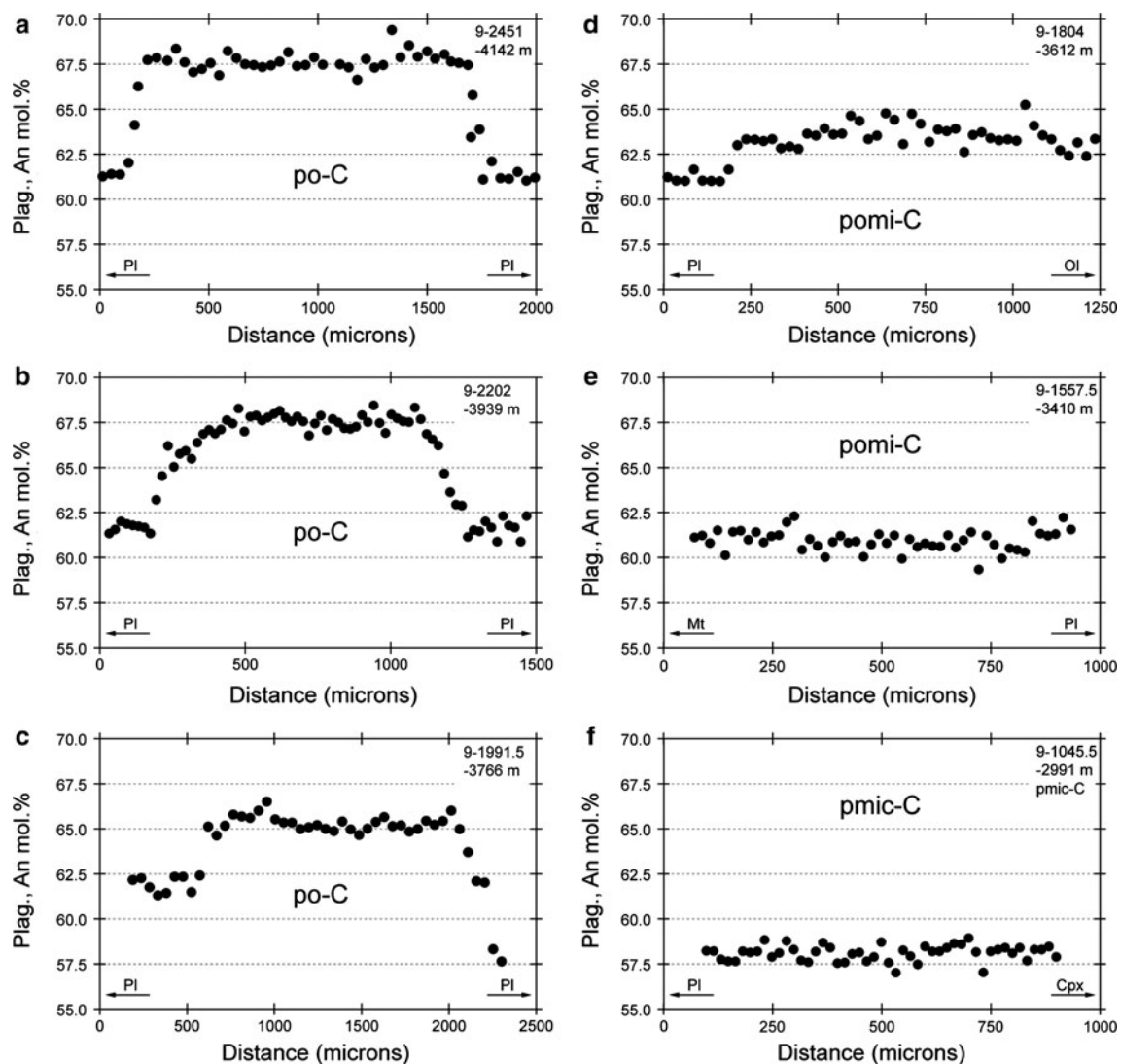
Fig. 4 Compositional profiles across representative grains of plagioclase throughout the Layered Series MCU I. The nature of the phase in contact with the analyzed plagioclase is indicated. The distance scale is from an arbitrary starting point, and only relative distances have any significance

throughout the MCU I. In magnetite, the Cr and V contents range, respectively, from 16 to 4,889 ppm and from 2,271 to 5,638 ppm and decrease continuously from the base of the pomi-C unit to the top of MCU I. Zr in magnetite is low and scatters between 1 and 7 ppm. Ilmenite shows a similar evolution for Cr (6–312 ppm) and V (125–1,024 ppm) and is significantly enriched in Zr (114–315 ppm).

Whole-rock trace element contents

The evolution of P_2O_5, Zr, Cr and V is illustrated in Fig. 7 and will be used here to quantify the amount of intercumulus melt in cumulate rocks (Table A3; Supplementary Materials). The P_2O_5 content is low in most samples of MCU I (from po-C to pmic-C; 0.02–0.10 wt%) and jumps at the base of the pomica-C unit (1.74–3.25 wt%),

corresponding to the onset of cumulus apatite crystallization (Fig. 7a). Figure 7b shows the details of P below the appearance of cumulus apatite. The po-C unit and, to a lesser extent, the pomi-C unit display large sample-to-sample fluctuations of P content ranging from less than 150 to 500 ppm at a scale of 30–250 m. In the pomic-C and pmic-C units, P contents are more homogeneous and relatively low (70–320 ppm). Zr ranges from 16 to 70 ppm and increases slightly from the po-C unit to the pmic-C unit, before decreasing in the pomica-C rocks (Fig. 7c). The whole-rock Cr content is low in the po-C unit (13–19 ppm; Fig. 7d) and jumps at the base of the pomi-C unit (137–345 ppm) before decreasing significantly in the upper part of this unit. It is then low to the top of MCU I (2–102 ppm). V is low in po-C rocks (51–86 ppm; Fig. 7e) and increases throughout the pomi-C unit (206–1,163 ppm),
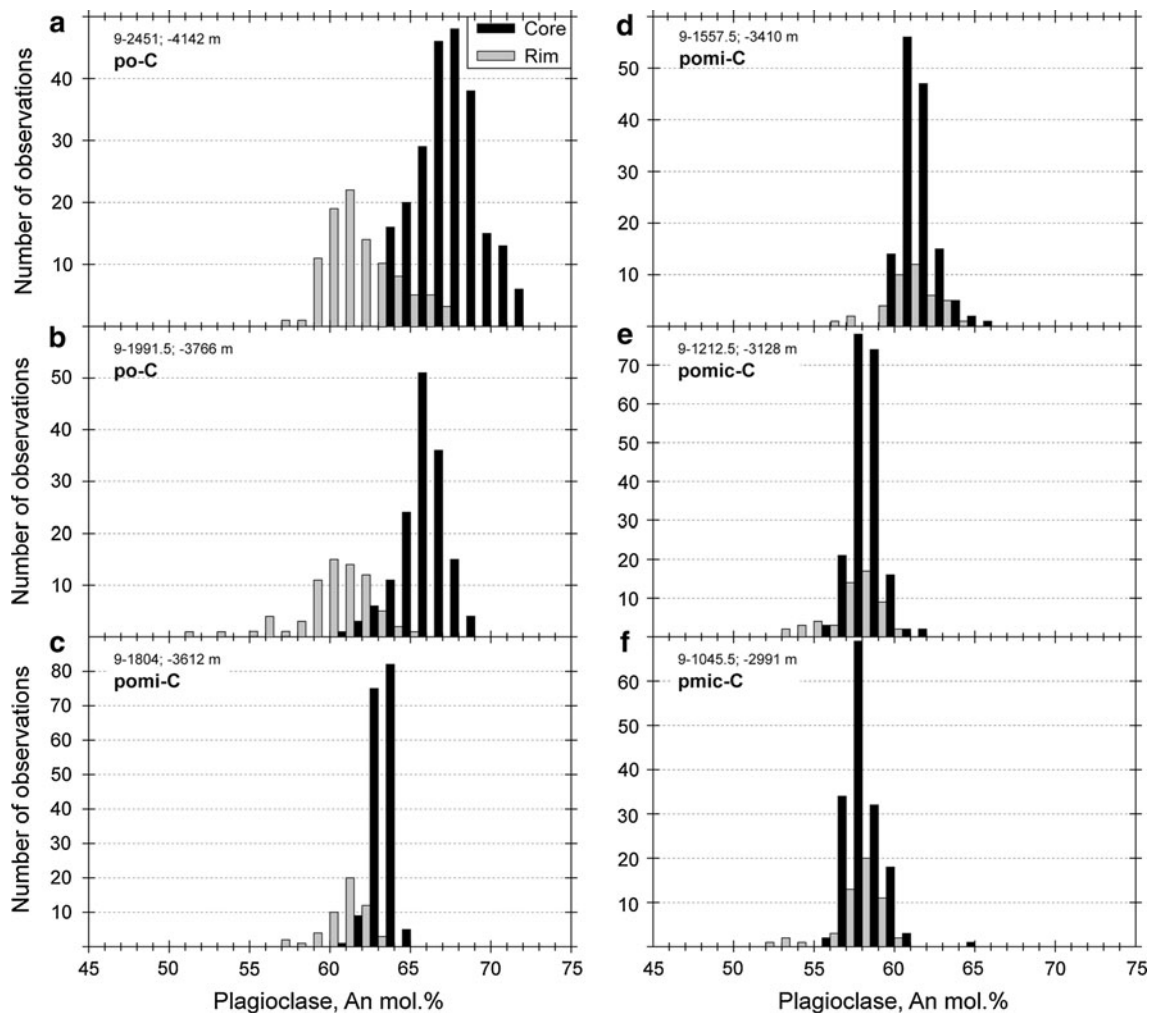
Fig. 5 Histograms of plagioclase compositions (An mol%) for 6 representative samples of the Sept Iles Layered Series MCU I

before decreasing continuously to the top of MCU I (pomic-C; pmic-C; pomica-C: 17–1,010 ppm). The increase in Cr and V at the base of the pomi-C is related to the appearance of cumulus Fe–Ti oxides. Saturation of these minerals results in a strong depletion of the Cr and V content of the liquid (Namur et al. 2011a), explaining the continuous decrease in the whole-rock Cr and V content toward the top of MCU I.

Whole-rock densities

Measured bulk-rock densities in the po-C unit are the lowest of MCU I and are highly homogeneous (2.78–3.01 g/cm^3; Fig. 7f; Table A3). After the appearance of cumulus Fe–Ti oxides, the bulk-rock densities increase significantly (2.91–3.94 g/cm^3). The calculated densities (see Electronic Supplementary Materials) of the cumulus crystal matrix at the liquidus temperature (2.81–3.96 g/cm^3) are relatively similar to the measured ones and mimic their stratigraphic variations.

Residual liquid versus stratigraphic height and physical properties of Sept Iles liquids

The Sept Iles parent magma is inferred to be a tholeiitic basalt (48 wt% SiO_2; 15 wt% FeOt; 0.4 wt% H_2O; Namur et al. 2010, 2011b). The liquid line of descent has the following characteristics: (1) Crystallization of troctolites drives the parent magma along a tholeiitic trend with FeOt-enrichment (up to 17 wt%) and slight SiO_2-depletion (down to 47 wt%); (2) saturation of Fe–Ti oxides and clinopyroxene drives the residual liquid along a FeOt-depletion and SiO_2-enrichment trend, ultimately leading to the formation of A-type granites.

The saturation of Fe–Ti oxides and apatite is estimated to occur, respectively, when the proportion of residual liquid in the magma chamber (F) is 0.86 and 0.52. Clinopyroxene saturates when F = 0.72 and the equilibrium plagioclase is An_{60} (Namur et al. 2011a). Namur et al. (2010) also defined the stratigraphic height (H, in m) in the Layered Series MCU I at which plagioclase and olivine
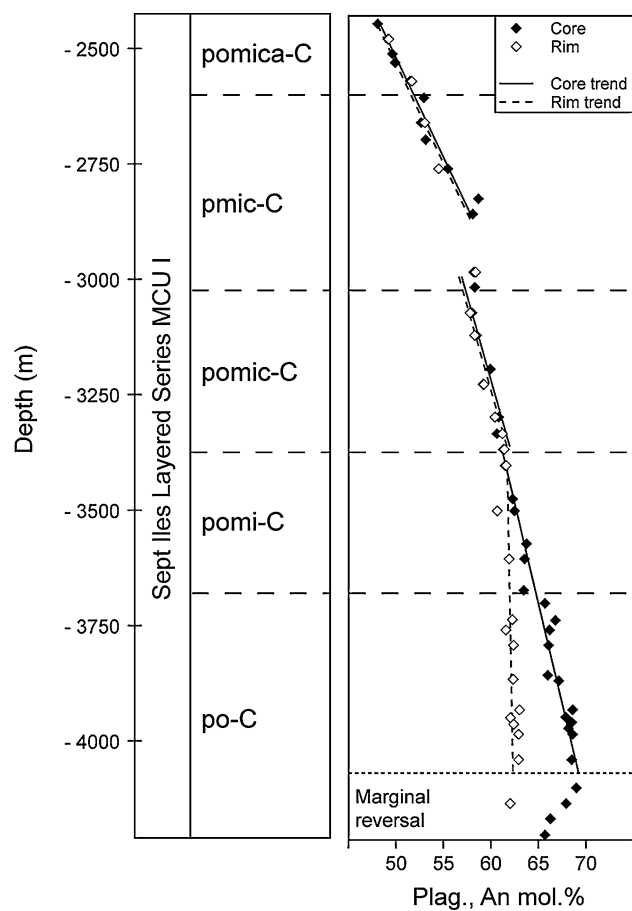
Fig. 6 Comparison of mean plagioclase core and rim compositions as a function of stratigraphic height in the Sept Iles Layered Series MCU I (see data in Table A1; Supplementary Materials). *Solid* and *dashed lines* represent linear regressions, respectively, for core and rim compositions

(−4,210 m), Fe–Ti oxides (−3,680 m), clinopyroxene (−3,375 m) and apatite (−2,575 m) become cumulus phases. By combining stratigraphic and residual liquid data, the proportion of residual liquid in the magma chamber can be calculated at each stratigraphic height with the equation:

$$F = 4 \times 10^{-7} H^2 - 5 \times 10^{-5} H + 0.1343 \quad (r^2 = 0.99) \tag{1}$$

Liquid density and viscosity calculations were performed, respectively, following the expressions of Bottinga and Weill (1970) and Giordano et al. (2008), with thermal expansion and compressibility data from Lange and Carmichael (1987), Kress and Carmichael (1991), Toplis et al. (1994), Lange (1997) and Ochs and Lange (1997; 1999). Liquidus temperatures were calculated using the relation between the melt MgO content and the temperature experimentally observed by Toplis and Carroll (1995), and the liquid FeO/Fe_2O_3 ratios were estimated by assuming fO_2 conditions along the FMQ

buffer (Namur et al. 2010). Liquid density increased from 2.70 to 2.75 during crystallization of po-C rocks and then decreased continuously down to 2.63 g/cm³ due to fractionation of Fe–Ti oxide-bearing cumulates (Fig. 8a; Table A4; Supplementary Materials). With differentiation, liquid viscosity increased continuously from 45 to 302 Pa.s (Fig. 8b; Table A4), values in good agreement with those measured on natural FeO-rich basalts (Sato 2005; Ishibashi and Sato 2007).

Intercumulus liquid fraction in cumulate rocks

Assumptions and methodology for calculation

The whole-rock composition of a cumulate sample is determined by the relative contributions of the crystallized intercumulus liquid and that of the cumulus crystal matrix. For an element i, it can be expressed by the following equation:

$$c_i^{WR} = X^{IL} c_i^{Liq} + \sum X^i c_i^j \tag{2}$$

with

$$\sum X^i = 1 - X^{IL} \tag{3}$$

where X^{IL} is the intercumulus melt fraction, c_i^{Liq} is the concentration of element i in the liquid, X^j is the modal fraction of the cumulus phase j in the cumulate and c_i^j is the concentration of element i in phase j.

Following Eq. 2, the proportion of intercumulus liquid (X^{IL}) can be determined using the concentration of an element i in the whole-rock (c^{WR}) when the concentration of i in the equilibrium melt (c^{Liq}) and in the crystal matrix ($\sum X^j c_i^j$) is estimated. The proportions of the different cumulus phases are however initially unknown and cannot be directly estimated from the bulk modal proportions due to the presence of intercumulus material. We have thus determined the relative proportions of the intercumulus liquid and the different cumulus phases by least-squares linear regression of Eq. 2. The bulk-rock composition (c^{WR}) of each sample, the equilibrium liquid composition (c^{Liq}) and the compositions of the cumulus phases (c^j) were used as input data. Mineral compositions used in Eq. 2 have been calculated for P, Zr, Cr and V using the liquid composition and appropriate partition coefficients. The latter were determined using Sept Iles liquid compositions at the appearance of each cumulus phase and trace element mineral compositions. Values are reported in Table A2 (Supplementary Materials) and are found to be very similar to those reported in the literature (e.g., Libourel 1999; Bindeman et al. 1998; Klemme and Blundy 2002; Aigner-Torres et al. 2007).
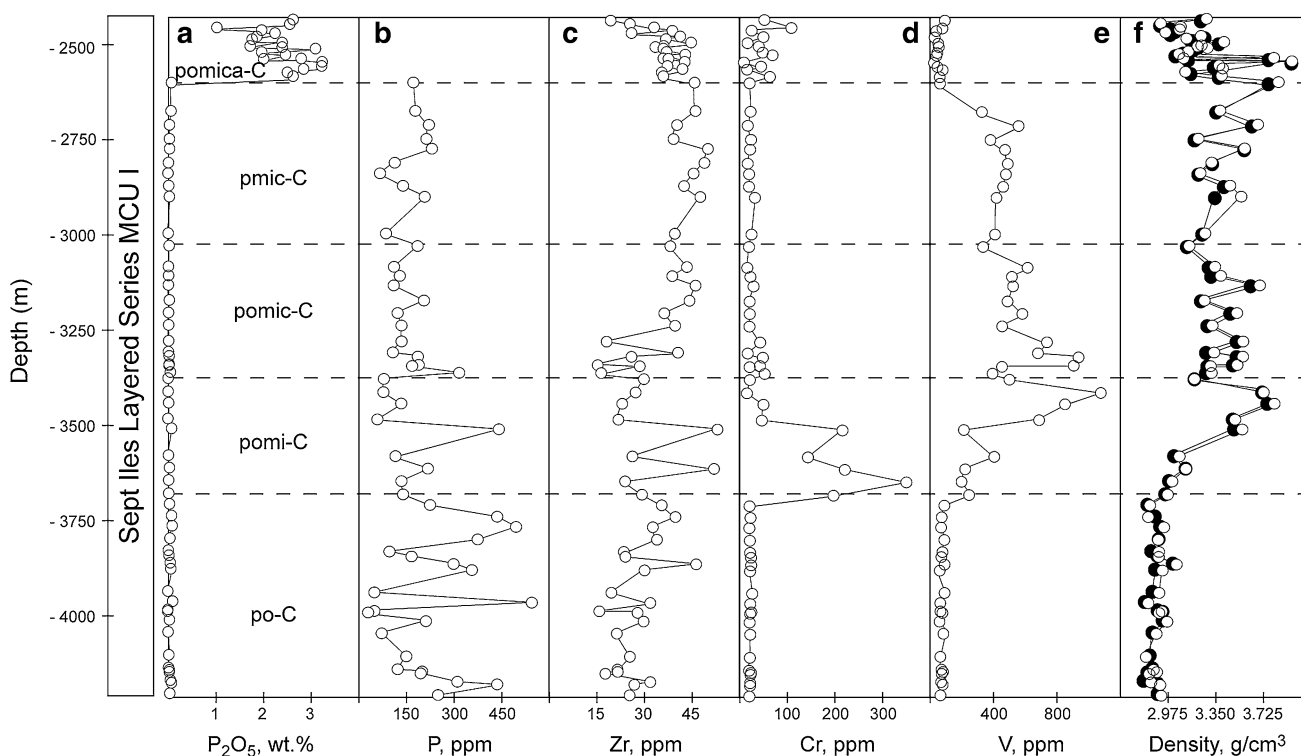
Fig. 7 Stratigraphic evolution of whole-rock trace element contents and density of cumulates from the Sept Iles Layered Series MCU I. *a* P$_2$O$_5$, *b* P, *c* Zr, *d* Cr, *e* V, *f* measured (*open circle*) and calculated (*filled circle*) densities of cumulate rocks. See Supplementary Materials for the methodology of calculation. Data listed in Table A3 (Supplementary Materials)

The evolution of the P$_2$O$_5$, Zr, Cr and V contents in the liquid has been calculated at each stage of fractionation using the Rayleigh fractionation model:

$$c_i^{\text{Liq}} = c_{i,0}^{\text{Liq}} \cdot f^{(D_i^{\text{Bulk}}-1)} \tag{4}$$

where c_i^{Liq} is the concentration of element i in the liquid at each step, $c_{i,0}^{\text{Liq}}$ is the concentration of element i in the liquid before each step, f is the mass fraction of each step relative to the mass of magma remaining in the chamber (F) and D_i^{Bulk} is the bulk partition coefficient of element i between the liquid and the crystal mush. The trace element composition of the Sept Iles parent magma was determined by Namur et al. (2010) and used as the starting composition in our calculations (P: 2,849 ppm; Zr: 152 ppm; Cr: 48 ppm; V: 241 ppm).

As a first approximation (iteration 1), the evolution of the liquid trace element content (c_i^{Liq}) was calculated using Eq. 4 by simulating perfect adcumulus growth (i.e., no intercumulus liquid is considered) and using cotectic proportions given by Namur et al. (2011a) for Sept Iles liquids. Using the calculated c_i^{Liq} curve with differentiation (see the example of P in Fig. 9a), X^{IL} values were determined by least-squares regression of Eq. 2 for each sample. Then, a second set of calculations of c^{Liq} (iteration 2) was performed by incorporating the effect of the intercumulus melt

(X^{IL} calculated from iteration 1) and assuming that its composition equals that of the main magma body, i.e., the partition coefficients equal unity. Including the effect of intercumulus melt in the calculations (iteration 2) only slightly reduces the liquid P$_2$O$_5$, Zr, Cr and V contents at each step of fractionation (see P in Fig. 9a). A second series of X^{IL} values was then calculated by least-squares regression of Eq. 2. Adding more iteration steps was tested, but the results are fundamentally the same as those presented here.

Intercumulus liquid fractions

X^{IL} values based on P content, which record the fraction of intercumulus liquid in the cumulate at the timing of apatite saturation, range from 0 to 0.154 (Fig. 9b). In the po-C unit and to a lesser extent in the lower part of the pomi-C unit, low and high X^{IL} values alternate at a scale of 30–250 m. In the upper part of MCU I (pomic-C and pmic-C units), X^{IL} values are much more homogeneous and relatively low (0–0.06). For cumulates in the po-C unit, X^{IL} values are high (0.10–0.28; Fig. 9c) when calculated using Zr, which is moderately compatible in ilmenite and strongly enriched in accessory phases such as zircon, although these accessory phases are extremely rare in Sept Iles cumulates. X^{IL} values are even higher when calculated using
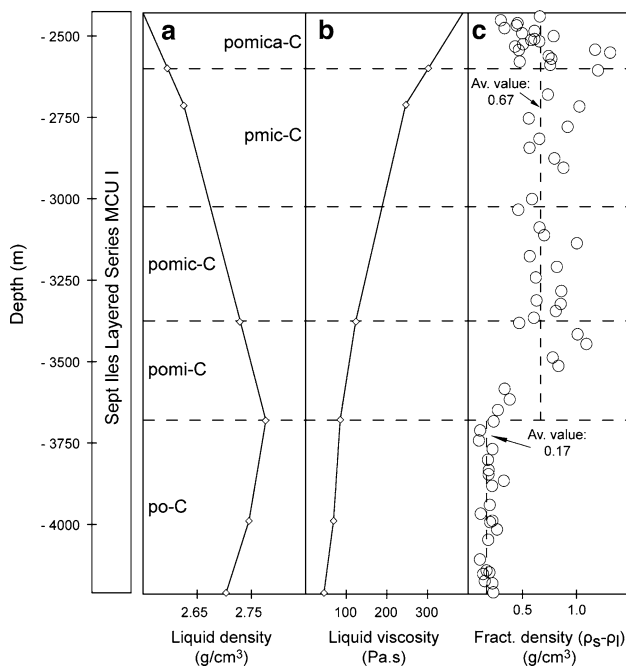
Fig. 8 Evolution of physical properties of the liquid and the crystal matrix as a function of stratigraphic height in the Layered Series MCU I. *a* Liquid density. *b* Liquid viscosity. *c* Fractionation density, representing the difference between the density of the crystal matrix calculated at the liquidus temperature and the density of the liquid

Cr (0.22–0.35; Fig. 9d) and V (0.20–0.23; Fig. 9e), which are strongly partitioned into Fe–Ti oxides.

Compaction and compositional convection: Theoretical models

Compaction

Compaction of the crystal mush expels interstitial liquid by squeezing it out of the mush due to deformation of a dense crystal matrix. Theoretical and experimental simulations together with studies of natural samples suggest high initial porosities for cumulate rocks (e.g., 40–70%; Shirley 1986; Philpotts and Carroll 1996; Philpotts et al. 1998; Jerram et al. 1996, 2003; Donev et al. 2004). In a crystal mush that accumulates at the floor of a magma chamber, the lower part is a compacting layer with a theoretical thickness given by δ_c (compaction length scale in m), while the upper part is not compacted. However, in most cases, the real thickness of the compacting layer (h in m) is smaller than the compaction length scale. With time, the compaction front moves upward through the crystal mush. The porosity decrease in the compacting layer results from the expulsion of the intercumulus melt and potentially from its progressive crystallization (Meurer and Boudreau 1998a; McKenzie 2011). Equations for compaction have been formulated by McKenzie (1984, 1985) and Sparks et al.

(1985) and are fully described in Supplementary Materials. They require the simplification of textural equilibrium between the crystals and the liquid in the crystal mush, i.e., there is no occlusion of the pores when the residual porosity is low (Hunter 1987; Mathez et al. 1997). Compaction is an efficient mechanism for producing adcumulate rocks when the velocity of liquid expulsion ($\omega - W$; m/s) is higher than the rate of crystal accumulation (Sparks et al. 1985).

Calculations of compaction of the Sept Iles crystal mush were performed assuming the following physical properties: (1) Two average grain sizes were used: 4 mm for the po-C unit and 2 mm for Fe–Ti oxide-bearing rocks (pomi-C to pomica-C); (2) by analogy with the Skaergaard intrusion, the crystal matrix viscosity is assumed to be between 10^{15} and 10^{17} Pa.s (Tegner et al. 2009; McKenzie 2011). Calculations were performed with a viscosity of 10^{15} Pa.s, which gives an upper estimate for the compaction efficiency; (3) the viscosity of the Sept Iles parent magma (45 Pa.s) was used for po-C cumulates and the liquid viscosity at the saturation of Fe–Ti oxides (85 Pa.s) was used for Fe–Ti oxide-bearing cumulates. Because the liquid viscosity increase during differentiation was not taken into account, the efficiency of compaction may have been overestimated; (4) fractionation densities ($\rho_s - \rho_l$) are relatively low in the po-C unit (0.09–0.32 g/cm³) and increase at the appearance of cumulus Fe–Ti oxides (from pomi-C to pomica-C; 0.22–1.31 g/cm³; Fig. 8c). Average fractionation densities for the different cumulus assemblages were used in compaction modeling (po-C: 0.17 g/cm³; pomi-C to pomica-C: 0.67 g/cm³).

While the expulsion of the intercumulus liquid from the crystal mush by compaction is a continuous phenomenon, equations currently available allow only stepwise modeling of this process (e.g., McKenzie 1984, 1985; Sparks et al. 1985; Shirley 1986). Each step corresponds to a reduction of porosity by a factor e (2.718), i.e., from ϕ_i, corresponding to the initial porosity before each step, to ϕ_i/e. Three steps were used here (ϕ: 0.6–0.22; ϕ: 0.22–0.08; ϕ: 0.08–0.03) and allow investigation of the potential efficiency of the compaction process from the initial porosity of Sept Iles cumulates (ϕ: 0.6) to the formation of adcumulate rocks (ϕ: <0.07).

Figure 10 shows that the velocity of liquid expulsion increases with the thickness of the crystal mush and decreases with the residual porosity. For po-C cumulates, the highest velocity of liquid migration is reached when the crystal mush is at least 31 m thick. In this case, the liquid is expelled at a rate of 2.5 m/year in the porosity interval 0.6–0.22; this rate decreases to 0.7 and 0.1 m/year for porosity intervals of 0.22–0.08 and 0.08–0.03, respectively (Fig. 10a). For Fe–Ti oxide-bearing cumulates, the highest velocity is achieved for a crystal mush ca. 10 m thick
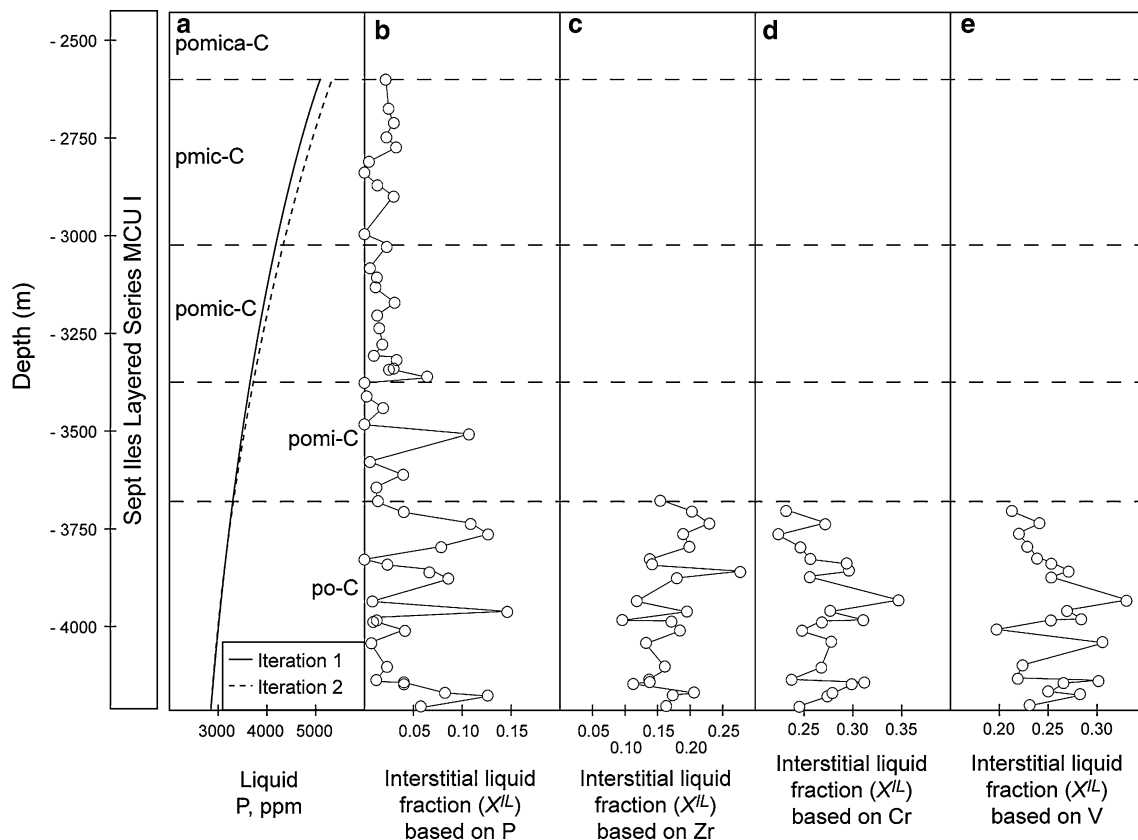
Fig. 9 *a* Calculated P content of residual liquids as a function of stratigraphic height. Calculations were carried out using the stepwise Rayleigh fractionation model (see text for details). The *solid curve* (iteration 1) assumes adcumulus differentiation, while the *dashed curve* (iteration 2) takes into account the presence of intercumulus melt in the crystal mush during fractionation. *b* Fraction of intercumulus melt calculated from the whole-rock and liquid P contents, see text for details on the methodology of calculation. *c* Fraction of intercumulus melt calculated using Zr. *d* Fraction of intercumulus melt calculated using Cr. *e* Fraction of intercumulus melt calculated using V

(Fig. 10b). The liquid is then expelled at a rate of 1.4 m/year in the porosity interval 0.6–0.22, decreasing to 0.4 and 0.05 m/year for porosity intervals of 0.22–0.08 and 0.08–0.03, respectively. The calculated values of crystal mush thickness for the Sept Iles MCU I are of the same order than those determined by Tegner et al. (2009) for the Skaergaard intrusion. There are however significantly lower than those calculated by McKenzie (2011) for the same intrusion. This contrast with the results of McKenzie (2011) simply results from the use of different values of initial porosity (0.6), crystal mush viscosity (10^{15} Pa s) and crystal sizes (2, 4 mm) that were considered more realistic for the Sept Iles layered intrusion.

Compositional convection

Saturation of Fe–Ti oxide minerals during differentiation of tholeiitic melt is responsible for a transition from a trend of increasing liquid density to one of decreasing liquid density (Sparks and Huppert 1984; Hunter and Sparks 1987; Namur et al. 2011b). When occurring in the pore space, saturation of Fe–Ti oxide minerals may locally decrease the density of the intercumulus melt to values lower than the density of the overlying magma in the main magma chamber. In this case, the intercumulus melt may be continuously expelled from the crystal mush through convective separation of the melt from growing crystals and replaced in the pore space by the overlying liquid. This compositional convection process maintains the pore melt at a constant composition (Tait et al. 1984).

The mathematical expressions for compositional convection were provided by Tait et al. (1984), Sparks et al. (1985) and Kerr and Tait (1986) and are described in Supplementary Materials. Instability occurs in the porous medium and leads to intercumulus melt convection when the dimensionless local solutal Rayleigh number (R_a) of the compositional porous boundary layer exceeds a critical value (25–80; Lapwood 1948; Nield 1968; Sparks et al. 1985; Tait and Jaupart 1992; Tait et al. 1992). Compositional convection is efficient at producing adcumulate rocks when the velocity of liquid flow (characteristic
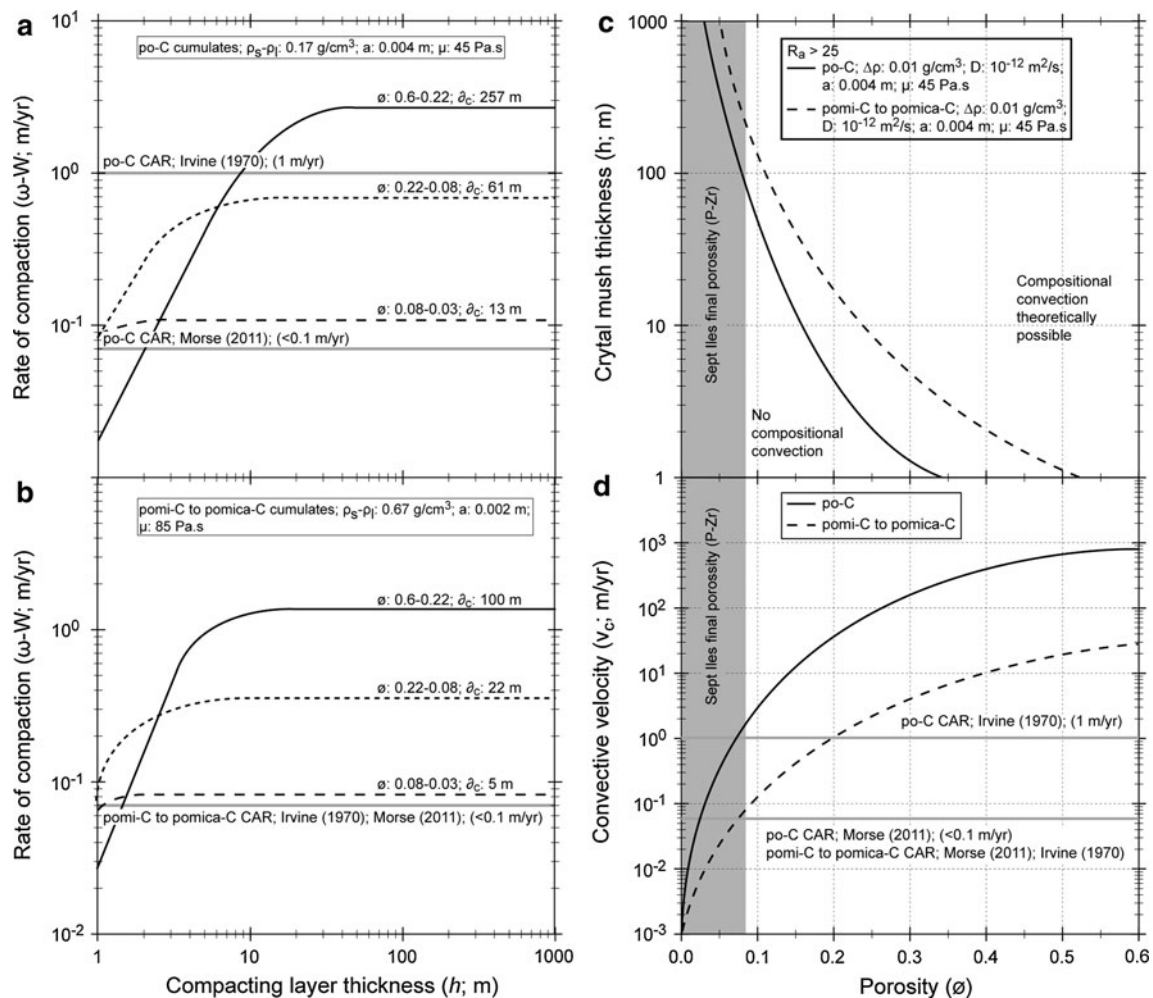
Fig. 10 Results of theoretical modeling of compaction and compositional convection in the crystal mush of the Sept Iles Layered Series MCU I. **a** Calculated rate of compaction of a crystal mush with plagioclase, olivine and liquid (po-C cumulates) as a function of the thickness of the compacting layer. The decrease in porosity due to compaction was modeled stepwise, and three steps are shown: ϕ: 0.60–0.22; 0.22–0.08; 0.08–0.03. The rates of crystal accumulation (CAR) estimated from the thermal analysis of Irvine (1970) and as discussed by Morse (2011) are also shown (see text for explanation). **b** Calculated rate of compaction of a crystal mush with plagioclase, Fe–Ti oxides, ±olivine, ±clinopyroxene, ±apatite and liquid (pomi-C to pomica-C cumulates) as a function of the thickness of the compacting layer. **c** Minimum crystal mush thickness allowing compositional convection to be operative ($R_a > 25$). Results are presented for Fe–Ti oxide-free cumulates (po-C) and for Fe–Ti oxide-bearing cumulates (pomi-C to pomica-C). **d** Evolution of the characteristic convective velocity (v_c) as a function of mush porosity. δ_c = compaction length-scale parameter, a = grain size radius, ϕ = porosity; $\rho_s - \rho_l$ = fractionation density (density of the crystal matrix − density of the melt); μ = viscosity of the liquid; D = diffusivity of the elements involved in the convection process; $\Delta\rho$ = density contrast across the boundary layer; μ = viscosity of the liquid

convective velocity; v_c) is higher than the rate of crystal accumulation (Kerr and Tait 1986).

Calculations were performed by considering the following physical parameters: (1) average grain sizes: 4 mm for the po-C unit and 2 mm for Fe–Ti oxide-bearing rocks (pomi-C to pomica-C); (2) magma viscosities of 45 Pa.s (po-C) and 85 Pa.s (pomi-C to pomica-C); (3) a density contrast across the boundary layer of 0.01 g/cm³ (Tait et al. 1984); (4) a melt diffusivity of 10^{-12} m²/s for the chemical species involved in the convection process (Hofmann 1980; Tait et al. 1984; Henderson et al. 1985).

The Rayleigh number (R_a) continuously decreases with the residual porosity, which controls the permeability, and with the thickness of the crystal mush (see Supplementary Materials). Considering a critical R_a value of 25, the minimal crystal mush thickness required to allow compositional convection at the lowest porosity values observed in Sept Iles rocks (ϕ: <0.1) is ca. 90 m for po-C cumulates and ca. 200 m for Fe–Ti oxide-bearing cumulates (Fig. 10c). The convective velocity of the intercumulus melt flow also decreases continuously with the residual porosity. Velocities as slow as 1 and 0.1 m/year are

calculated, respectively, for po-C and Fe–Ti oxide-bearing cumulates (pomi-C to pomica-C) at the lowest porosity values of Sept Iles cumulates (Fig. 10d). In contrast to what is calculated here, it is of interest to note that Morse (1982, 1986, 1988) suggested that compositional convection could be an operative mechanism even if the crystal mush is only a few cm thick.

Discussion

Efficiency of compaction and compositional convection

Insight from theoretical models

The low fractions of intercumulus liquid calculated in the previous sections indicate that most of the interstitial liquid was expelled from the crystal mush or exchanged by liquid from the main magma chamber during solidification of the Sept Iles cumulates. An immobile intercumulus melt would have reached saturation in Fe–Ti oxides, apatite and zircon in each sample, and X^{IL} values calculated using P, Zr, Cr and V should therefore give similar results approaching 0.6, which is obviously not the case. However, po-C cumulates show evidence for crystallization of intercumulus liquid such as plagioclase zoning and contrasted X^{IL} when calculated on the basis of elements incorporated in Fe–Ti oxides (Cr, V and Zr) or in apatite (P). This indicates that the intercumulus liquid was not expelled very efficiently at the onset of formation of the cumulus framework or that it stayed temporarily immobile during the solidification history of the crystal mush. The very low X^{IL} values calculated on the basis of P for all the rocks nevertheless indicate that the last stage of liquid migration only stopped when the residual porosity was very low (ϕ: <0.1). For such low porosity values, it is reasonable to suggest that the percolation threshold was reached and that X^{IL} values calculated on the basis of P represent the actual trapped liquid fractions (Cheadle et al. 2004; Tegner et al. 2009).

The ability of compaction and compositional convection in producing intercumulus liquid migration at the lowest porosity values observed in Sept Iles cumulates depends on two parameters that are largely unknown: (1) the thickness of the crystal mush and (2) the rate of crystal accumulation at the floor of the magma chamber (Fig. 10). Concerning the crystal mush thickness, it has been calculated that at least 10 and 90–200 m are required to allow, respectively, compaction and compositional convection to be efficient (Fig. 10). The thickness of the crystal mush at the floor of mafic intrusions is generally thought to be in the range of tens to hundreds of meters (Sparks et al. 1985; Tait and Jaupart 1989, 1992; Marsh 1996; Philpotts et al. 1996; Mathez et al. 1997; MacLeod and Yaouancq 2000).

However, recent studies based on plagioclase-plagioclase-clinopyroxene dihedral angles suggest that it may be thinner than 10 m (Holness et al. 2007c, 2009, 2011). Another argument in favor of thin crystal mushes in mafic layered intrusions is the absence of significant deformation of the layering beneath blocks (basaltic, anorthositic and troctolitic) in the Layered Series of the Skaergaard intrusion (Irvine et al. 1998). However, given the poor knowledge of crystal mush rheology (Pinkerton and Norton 1995; Dimanov et al. 1998), constraining the crystal mush thickness using the deformation of the layering is presently highly speculative. Comparison of our calculations with estimates from the literature suggests that the highest proposed values for crystal mush thickness (e.g., hundreds of meters) would theoretically allow both compaction and compositional convection as mechanisms of intercumulus liquid migration, while the lowest values (less than 10 m) would only allow compaction to be operative.

The rate of crystal accumulation at the base of the Sept Iles layered intrusion may be estimated from the thermal analysis of Irvine (1970) for large magma chambers. Assuming a rate of crystal accumulation of 19.6 m/year$^{1/2}$, a value considered realistic for the Bushveld, Dufek and Skaergaard intrusions (Irvine 1970; Tegner et al. 2009), the estimated accumulation rate is high during the initial stages of crystallization and decreases continuously with time following a second-order polynomial curve. By approximating this curve as a series of line segments, crystal accumulation is calculated to be ca. 1 m/year for the po-C unit, decreasing continuously upwards (pomi-C: 0.3 m/year; pomic-C: 0.1 m/year; pmic-C: 0.06 m/year; pomica-C: 0.02 m/year). However, the rather high crystal accumulation rates, especially for po-C cumulates, contrast with the values commonly accepted for crystal accumulation rate at the floor of mafic layered intrusions (<0.1 m/year; Morse 1979, 2011, Sparks et al. 1985; Nielsen 2004). In the assumption of a high accumulation rate for po-C cumulates (e.g., 1 m/year), compaction cannot be efficient at expelling the intercumulus melt when the residual porosity is lower than 0.22 (Fig. 10a). However, such a high rate of crystal accumulation has no effect on the efficiency of compositional convection (Fig. 10d). In contrast, for lower rates of crystal accumulation (<0.1 m/year), compaction of the crystal mush and compositional convection may both operate even at the lowest porosity values observed in Sept Iles cumulates (ϕ: <0.1).

In the absence of accurate estimates for the thickness of the crystal mush, the rate of crystal accumulation at the floor of the magma chamber and the efficiency of compositional convection in very thin crystal mushes (Tait et al. 1984; Morse 1986, 1988; Tait and Jaupart 1989), theoretical models cannot be used to unambiguously determine the relative efficiency of compaction and

compositional convection at segregating the intercumulus melt from the Sept Iles cumulates. In the following discussion, whole-rock geochemical data and plagioclase compositional profiles will be used to constrain the relative contributions of these two processes in producing meso- to ortho-cumulates with low P content in the po-C unit and adcumulates in the upper part of MCU I.

Insight from intercumulus liquid fractions

The contrasting fractions of intercumulus liquid (X^{IL}) in po-C rocks when calculated on the basis of Cr, V and Zr on the one hand and on the basis of P on the other hand may be used to constrain the mechanisms of intercumulus melt flow within the cumulus crystal framework. In po-C cumulates, X^{IL} values are high when calculated using elements strongly partitioned into Fe–Ti oxides (Cr and V: ca. 0.25–0.35; Zr: 0.10–0.25) and do not show any systematic evolution with stratigraphic height. In contrast, X^{IL} values are low when calculated using P (0.0–0.15, with most samples below 0.10). Contrasting X^{IL} values derived from elements with different degrees of bulk compatibility are traditionally interpreted as evidence of crystallization of the intercumulus melt during liquid flow caused by compaction (Meurer and Boudreau 1998a). However, these combined processes cannot explain the relatively constant X^{IL} values calculated using Cr, V and Zr for all po-C samples. With increasing stratigraphic height in the po-C unit, the liquid that is initially located between cumulus crystals becomes progressively more evolved and compositionally close to saturation in Fe–Ti oxides. Consequently, the degree of intercumulus liquid differentiation and the time available for liquid expulsion before local saturation of Fe–Ti oxides continuously decreases upwards. In the hypothesis of crystallization during liquid flow, the fraction of intercumulus liquid at saturation of Fe–Ti oxides must thus increase upwards and approach the value of the initial porosity (ϕ: 0.5–0.7; Fig. 11), while relatively constant values are observed (ϕ: 0.3; Fig. 11). Consequently, we suggest that a mechanism initially operated to reduce the porosity to a critical value of ca. 0.3 and then stopped. This value was reached before local saturation of Fe–Ti oxides in the intercumulus melt, assuming that the liquid becomes highly depleted in Cr and V soon after the saturation of magnetite (Namur et al. 2010, 2011a; Fig. 7). This suggests that the initial velocity of liquid expulsion was high (McKenzie 2011). Given the increase in residual melt density before the saturation of Fe–Ti oxides (Fig. 8), compositional convection cannot have operated and compaction of the crystal mush is therefore thought to be the only possible mechanism to reduce the porosity to a value of 0.3.

The termination of compaction at a residual porosity of 0.3 is presumably related to the velocity of liquid expulsion falling below the rate of crystal accumulation. The very low X^{IL} values calculated on the basis of P nevertheless indicate that another process occurred to expel or exchange much of the residual intercumulus melt after the local saturation of Fe–Ti oxides. The decrease in residual melt density after the crystallization of Fe–Ti oxides may theoretically have allowed compositional convection to operate. This process is efficient even when the rate of crystal accumulation is as high as 1 m/year (Fig. 10d). Compositional convection continuously exchanged intercumulus melt with the overlying melt, thereby maintaining a constant pore liquid composition. This liquid composition was close to that of the first Fe–Ti oxide-saturated melt and was therefore not saturated in apatite, thus explaining the very low X^{IL} values calculated on the basis of P. Crystallization of the intercumulus melt contemporaneously with compositional convection reduced the residual porosity until the percolation threshold was reached (ϕ: <0.1;
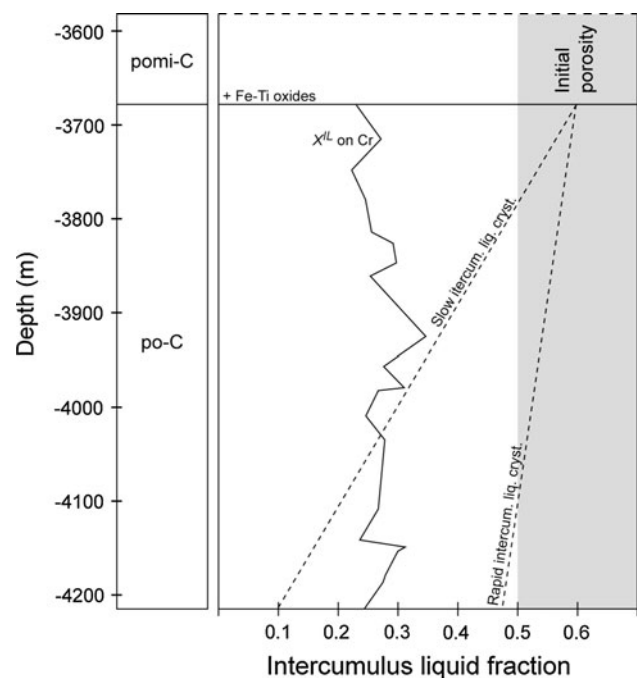

Fig. 11 Theoretical model showing the evolution of the proportion of intercumulus melt recorded by elements strongly partitioning into Fe–Ti oxides (e.g., Cr) in the po-C unit. Crystallization of the intercumulus liquid occurs as compaction expels the liquid from the crystal mush. Two theoretical curves are shown: (1) slow rate of intercumulus liquid crystallization where the proportion of intercumulus liquid that reached Fe–Ti oxide-saturation is mainly controlled by the rate of liquid expulsion during compaction; (2) rapid intercumulus liquid crystallization where the proportion of intercumulus liquid that reached Fe–Ti oxide-saturation is mostly controlled by the rate of liquid crystallization. The calculated proportion of intercumulus melt (based on whole-rock Cr content) that reached Fe–Ti oxide-saturation in po-C cumulates is shown for comparison

Cheadle et al. 2004). At this stage, liquid exchange ceased and the trapped liquid evolved to the saturation of late-stage phases such as apatite, thus explaining the presence of minor P in whole-rock po-C cumulates.

Insight from plagioclase compositional profiles

The geochemical consequences of compaction and compositional convection can be observed in the zoning patterns of minerals with low diffusivity rates, such as plagioclase. While the constant core composition is well known to result from near isothermal crystallization in the magma body in slow cooling conditions, rim compositions will be highly dependent on postcumulus processes. Compaction may result in two different compositional profiles: (1) If efficient compaction occurs, the intercumulus melt can be expelled as soon as the cumulus framework is formed. The cumulus plagioclase core is then not surrounded by any intercumulus rim; (2) if the velocity of liquid expulsion is slower than the rate of intercumulus liquid crystallization, the cumulus plagioclase core is surrounded by an intercumulus rim increasingly enriched in albite. Compositional convection may also have two different effects on zoning patterns. They depend on the timing of convection onset: (1) If crystallization of the first intercumulus phases locally decreases the density of the melt, the core will be surrounded by a unzoned intercumulus rim, which is virtually indistinguishable from the absence of postcumulus overgrowth; (2) if crystallization of the first intercumulus phases locally increases the melt density, compositional convection does not occur and the core is surrounded by an intercumulus rim increasingly enriched in albite. When Fe–Ti oxides saturate in the pore space, the intercumulus melt density starts to decrease (Sparks and Huppert 1984; Hunter and Sparks 1987; Namur et al. 2011b). In this case, compositional convection may begin and the pore space at the base of the mush can thus be filled up with a liquid of uniform composition. Crystallization of this liquid results in the formation of an external intercumulus rim of constant composition around plagioclase crystals.

Plagioclase crystals from the po-C unit and the lower part of the pomi-C unit are all characterized by a relatively primitive core ($An_{>61}$) surrounded by an intercumulus rim with two different compositional zones: (1) a thin internal zone of decreasing An content outward and (2) a variably thick external zone buffered at $An_{61\pm1}$ (Fig. 4). The internal rim may be explained by intercumulus liquid crystallization during compaction (Meurer and Boudreau 1998a), but the external rim of constant composition can only be explained by compositional convection keeping the intercumulus melt at a constant composition. This mechanism began to operate when the intercumulus melt became saturated in a plagioclase of composition An_{61}. Interestingly, in the Layered Series, cumulus plagioclase with a composition of An_{61} occurs in the middle part of the pomi-C unit (Fig. 6). This indicates that the external rims on plagioclase from the po-C unit and the lower part of the pomi-C unit were in equilibrium with an intercumulus liquid that was saturated in Fe–Ti oxides but not yet in clinopyroxene (Namur et al. 2011a). The density maximum of Sept Iles liquids occurs at the saturation of Fe–Ti oxides (Fig. 8), when plagioclase has a composition of An_{63} (Fig. 6). There is thus a significant offset between the saturation of Fe–Ti oxides, i.e., the initiation of decreasing liquid density, and the start of compositional convection. The explanation for this offset is that a sufficient density difference between the intercumulus liquid and the overlying liquid must be reached to initiate compositional convection (Toplis et al. 2008).

General model for the mobility of intercumulus melt

Geochemical data outlined above allow us to propose a 3-stage model for the complete solidification of the po-C cumulates:

1. The parental magma ($\rho = 2.70$ g/cm^3) starts to crystallize plagioclase and olivine cumulates with an initial porosity of 0.5–0.7 (Fig. 12a). The plagioclase crystallizing at the bottom of the mush has a composition of ca. 67 mol% An (Fig. 12a);

2. The intercumulus melt initially crystallizes plagioclase and olivine, which causes an increase in the liquid density (Fig. 12b). Crystallization of the intercumulus melt is faster than that in the main magma body, which has the effect of producing a stable liquid density distribution within the magma chamber. Compaction of the crystal mush occurs together with minor contemporaneous crystallization of the intercumulus melt (McKenzie 2011); both processes contribute to progressively reduce the porosity to ca. 0.3 (Fig. 12b). During this stage, the intercumulus melt crystallizes a thin plagioclase overgrowth evolving outward from An_{67} to An_{61} (Fig. 12b);

3. Saturation of intercumulus Fe–Ti oxides at the bottom of the crystal mush reduces the density of pore liquid, thus producing an unstable distribution of liquid densities within the crystal mush, which initiates compositional convection (Fig. 12c). The liquid in the main magma body is not involved in the convection process because the dense intercumulus melt in the upper part of the crystal mush acts as a physical barrier. Convection allows the liquid at the bottom of the crystal mush to maintain a uniform composition and to crystallize external plagioclase rims with constant composition (An_{61}; Fig. 12c). With

Fig. 12 Schematic model for solidification of troctolites (po-C cumulates) in the Sept Iles Layered Series MCU I. **a** Crystallization of the first plagioclase and olivine grains (po-C cumulates). Plagioclase has a composition of 67 mol% An. **b** Compaction of the crystal mush, together with crystallization of the intercumulus melt. At this stage, the intercumulus melt is saturated in plagioclase and olivine only. Cumulus plagioclase grains at the base of the mush have a core of An_{67} composition that is surrounded by an intercumulus rim increasingly enriched in the albite component. **c** Initiation of compositional convection due to the saturation of intercumulus Fe–Ti oxides at the bottom of the crystal mush. The porosity reduction in this part of the mush is achieved by crystallization of the intercumulus melt, which produces external plagioclase rims buffered at An_{61}
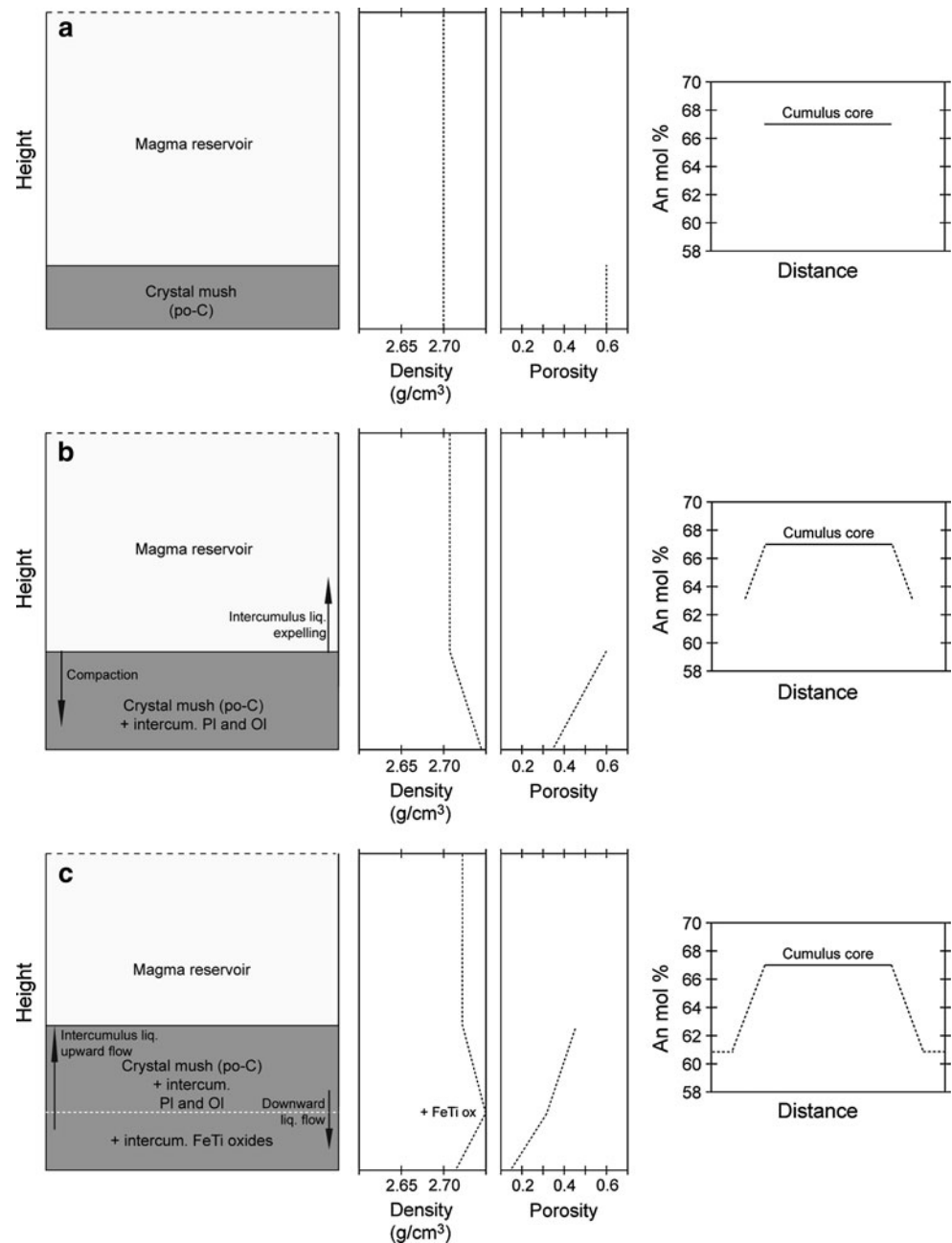
compaction no longer operating, the porosity reduction of the crystal mush results entirely from this in situ crystallization of the intercumulus melt. When the porosity becomes very low (<0.1), the percolation threshold is reached and the intercumulus liquid becomes effectively trapped (Cheadle et al. 2004). Differentiation of trapped liquid leads to the saturation of apatite, thus explaining the low amounts of P in po-C samples and the outermost rim with low An content (<An_{60}) around some plagioclase crystals.

The adcumulate nature of Fe–Ti oxide-bearing cumulates (pomi-C to pomica-C) may be explained by

compaction of the crystal mush, which is facilitated by (1) the high density contrast between the cumulus crystal matrix and the equilibrium melts and (2) the decreasing rate of crystal accumulation from base to top in the magma chamber (Irvine 1970). The saturation of Fe–Ti oxides in the main magma body also allows compositional convection to operate as soon as the cumulus framework forms. In contrast to po-C rocks, where compaction and compositional convection occur successively, it is highly probable that these two processes occur together during the solidification of Fe–Ti oxide-bearing cumulates.

Fluid flow dynamics

The distribution of the last fraction of intercumulus melt in Sept Iles cumulates, as recorded by the whole-rock P content, is significantly different in po-C rocks and Fe–Ti oxide-bearing rocks (pomi-C to pmic-C). In po-C, the distribution of P is heterogeneous, and high and low values alternate at a scale of 30–250 m (Fig. 9b). In pomi-C to pmic-C cumulates, the distribution of the whole-rock P content is less variable, suggesting that the last fraction of intercumulus melt was homogeneously distributed throughout the mush.

Little direct information is available in the literature concerning fluid flow dynamics in cumulate rocks from layered intrusions (e.g., Irvine 1980; Larsen and Brooks 1994). However, studies of rocks from the upper mantle and experimental simulations of liquid migration in porous media have shown that liquid may ascend a partly molten rock column (e.g., peridotite) either through a pervasive porous flow or through a channelized flow (Kelemen et al. 1995, 1997; Ertan and Leeman 1996; Beccaluva et al. 2004; Van Den Bleeken et al. 2010). In the mantle wedge, whether the liquid migrates as a porous flow or as a channel flow depends on processes of reactive infiltration-dissolution (Daines and Kohlstedt 1994; Morgan and Liang 2003) and also on the grain size of the porous medium (Wark and Watson 2000). Planar mineral fabrics such as lamination are also likely to exert a control on the fluid flow dynamics (Vanderhaege 2001). Here, we interpret the contrasting distribution of the last fractions of intercumulus melt in cumulates from the Sept Iles MCU I as resulting from two mechanisms of liquid migration: as channels in po-C cumulates and as a porous flow in Fe–Ti oxide-bearing cumulates. In po-C cumulates, we have shown that compaction initially occurs until the porosity reaches a value of 0.3. The final porosity reduction is then achieved by crystallization of the intercumulus melt during fluid flow exchange by compositional convection. Compositional convection is well known to frequently develop channel flow during liquid migration (Bédard et al. 1992; Tait et al. 1992; Worster 1992; Emms and Fowler 1994; Morse 2008), especially in rocks where minerals show contrasted grain sizes, such as troctolites (Wark and Watson 2000). Channelization of the intercumulus liquid is thus interpreted as being responsible for the heterogeneous distribution of P in po-C cumulates. In Fe–Ti oxide-bearing cumulates (pomi-C to pomica-C), the porosity reduction may result from compaction of the crystal mush, compositional convection or a combination of both. The homogeneous distribution of the last fraction of intercumulus melt within the pore space indicates that compaction may have been the major process of porosity reduction, as it is generally accepted that compaction results in porous flow

liquid migration rather than channelization of the liquid (McKenzie 1984; Scott and Stevenson 1986; Gutierrez et al. 2002; Chauveau and Kaminski 2008). The dominant effect of compaction in Fe–Ti oxide-bearing cumulates is moreover illustrated by the high aspect ratio of their plagioclase crystals (Fig. 3b) and the development of a very well-defined mineral lamination (Fig. 2), two features generally interpreted as resulting from crystallization under uniaxial stress during compaction (Meurer and Boudreau 1998b). Mineral lamination is also supposed to act as a mechanical guide for porous fluid migration (Vanderhaege 2001).

Conclusions

Stratigraphic evolution of whole-rock trace element contents (Cr, V, Zr and P) and detailed plagioclase compositional profiles (An content) in cumulates of the Sept Iles layered intrusion have been used to show that both compaction and compositional convection operate to expel the intercumulus melt from the crystal network or to exchange it with the liquid from the main magma chamber. However, the relative efficiency of these two processes varies with differentiation. Before the appearance of Fe–Ti oxides in the intercumulus assemblage, compositional convection cannot operate due to a stable liquid density distribution within the crystal mush. The initial porosity reduction thus results from compaction of the crystal mush until the residual porosity reaches 30%. The onset of compositional convection due to the decreasing density of the pore liquid then starts to exchange the intercumulus liquid with that of the main magma chamber. Compositional convection is confirmed by the thick external rims of plagioclase buffered to An_{61}, which suggest a constant composition for the solidifying intercumulus liquid. The composition of the plagioclase rims also indicates that compositional convection starts rapidly after the local saturation of Fe–Ti oxides in the pore space, as a consequence of decreasing intercumulus liquid density. In Fe–Ti oxide-bearing gabbros, intercumulus liquid migration results from a combination of compaction and simultaneous compositional convection. The homogeneously low trapped liquid fraction in these rocks suggests that liquid migration has occurred as a porous flow, which contrasts with the heterogeneous distribution of P in troctolites that suggests channelized liquid flow.

References

Aigner-Torres M, Blundy J, Ulmer P, Pettke T (2007) Laser Ablation ICPMS study of trace element partitioning between plagioclase and basaltic melts: an experimental approach. Contrib Mineral Petrol 153:647–667

Beccaluva L, Bianchini G, Bonadiman C, Siena F, Vaccaro C (2004) Coexisting anorogenic and subduction-related metasomatism in mantle xenoliths from the Betic Cordillera (Southern Spain). Lithos 75:67–87

Bédard JH, Kerr RC, Hallworth MA (1992) Porous sidewall and sloping floor crystallization experiments using a reactive mush: implications for the self-channelization of residual melts in cumulates. Earth Planet Sci Lett 111:319–329

Bindeman IN, Davis AM, Drake MJ (1998) Ion microprobe study of plagioclase-basalt partition experiments at natural concentration levels of trace elements. Geochim Cosmochim Acta 62:1175–1193

Bottinga Y, Weill DF (1970) Densities of liquid silicate systems calculated from partial molar volumes of oxide components. Am J Sci 269:169–182

Campbell IH (1978) Some problems with the cumulus theory. Lithos 11:311–323

Charlier B, Vander Auwera J, Duchesne JC (2005) Geochemistry of cumulates from the Bjerkreim-Sokndal layered intrusion (S. Norway). Part II: REE and the trapped liquid fraction. Lithos 83:255–276

Chauveau B, Kaminski E (2008) Porous compaction in transient creep regime and implications for melt, petroleum, and CO_2 circulation. J Geophys Res 113:B09406. doi:10.1029/2007JB005088

Cheadle MJ, Elliott MT, McKenzie D (2004) Percolation threshold and permeability of crystallizing igneous rocks: the importance of textural equilibrium. Geology 32:757–760

Daines MJ, Kohlstedt DL (1994) The transition from porous to channelized due to melt/rock reaction during melt migration. Geophys Res Lett 21:145–148

Dimanov A, Dresen G, Wirth R (1998) High-temperature creep of partially molten plagioclase aggregates. J Geophys Res 103:9651–9664

Donev A, Cisse I, Sachs D, Variano EA, Stillinger FH, Connelly R, Torquato S, Chaikin PM (2004) Improving the density of jammed disordered packings using ellipsoids. Science 303:990–993

Emms PW, Fowler AC (1994) Compositional convection in the solidification of binary alloys. J Fluid Mech 262:111–139

Ertan IE, Leeman WP (1996) Metasomatism of Cascades subarc mantle: evidence from a rare phlogopite orthopyroxenite xenolith. Geology 24:451–454

Giordano D, Russell JK, Dingwell DB (2008) Viscosity of magmatic liquids: a model. Earth Planet Sci Lett 271:123–134

Gutierrez MS, Asce M, Lewis RW (2002) Coupling of fluid flow and deformation in underground formations. J Eng Mech 128:779–787

Henderson P, Nolan J, Cunningham GC, Lowry RK (1985) Structural controls and mechanisms of diffusion in natural silicate melts. Contrib Mineral Petrol 89:263–272

Higgins MD (1991) The origin of laminated and massive anorthosite, Sept Iles layered intrusion, Quebec, Canada. Contrib Mineral Petrol 106:340–354

Higgins MD (2005) A new interpretation of the structure of the Sept Iles Intrusive Suite, Canada. Lithos 83:199–213

Higgins MD, van Breemen O (1998) The age of the Sept Iles layered mafic intrusion, Canada: implications for the late Neoproterozoic/Cambrian history of southeastern Canada. J Geol 106:421–431

Hofmann AW (1980) Diffusion in natural silicate melts: a critical review. In: Hargraves RB (ed) Physics in magmatic processes. Princeton, New Jersey, pp 385–418

Holness MB (2005) Spatial constraints on magma chamber replenishment events from textural observations of cumulates: the Rum Layered Intrusion, Scotland. J Petrol 46:1585–1601

Holness MB, Nielsen TF, Tegner C (2007a) Textural maturity of cumulates: a record of chamber filling, cooling rate and large-scale convection in mafic layered intrusions. J Petrol 48:141–157

Holness MB, Anderson AT, Martin VM, Maclennan J, Passmore E, Schwindinger K (2007b) Textures in partially solidified crystalline nodules: a window into the pore structure of slowly cooled mafic intrusions. J Petrol 48:1243–1264

Holness MB, Tegner C, Nielsen TF, Stripp G, Morse SA (2007c) A textural record of solidification and cooling in the Skaergaard intrusion, East Greenland. J Petrol 48:2359–2377

Holness MB, Tegner C, Nielsen TF (2009) Constraining the thickness of the crystal mush in layered mafic intrusions. AGU Fall Meeting, V13F-05

Holness MB, Stripp G, Humphreys MC, Veksler IV, Nielsen TF, Tegner C (2011) Silicate liquid immiscibility within the crystal mush: late-stage magmatic microstructures in the Skaergaard intrusion, East Greenland. J Petrol 52:175–222

Hunter RH (1987) Textural equilibrium in layered igneous rocks. In: Parsons I (ed) Origins of igneous layering. Dordrecht, Reidel, pp 473–503

Hunter RH, Sparks RS (1987) The differentiation of the Skaergaard intrusion. Contrib Mineral Petrol 95:451–461

Huppert HE, Sparks RS (1984) Double-diffusive convection due to crystallization in magmas. Ann Rev Earth Planet Sci 12:11–37

Irvine TN (1970) Heat transfer during solidification of layered intrusions. I. Sheets and sills. Can J Earth Sci 7:1031–1061

Irvine TN (1980) Magmatic infiltration metasomatism, double-diffusive fractional crystallization, and adcumulus growth in the Muskox and other layered intruions. In: Hargraves RB (ed) Physics of magmatic processes. Princeton University Press, Princeton, pp 325–383

Irvine TN (1982) Terminology for layered intrusions. J Petrol 23:127–162

Irvine TN, Andersen JC, Brooks CK (1998) Included blocks (and blocks within blocks) in the Skaergaard intrusion: geologic relations and the origins of rhythmic modally graded layers. GSA Bull 110:1398–1447

Ishibashi H, Sato H (2007) Viscosity measurements of subliquidus magmas: alkali olivine basalt from the Higashi-Matsuura district, Southwest Japan. J Volcanol Geotherm Res 160:223–238

Jerram DA, Cheadle MJ, Hunter RH, Elliott MT (1996) The spatial distribution of grains and crystals in rocks. Contrib Mineral Petrol 125:60–74

Jerram DA, Cheadle MJ, Philpotts AR (2003) Quantifying the building blocks of igneous rocks: are clustered crystal frameworks the foundation? J Petrol 44:2033–2051

Kelemen PB, Shimizu N, Salters VJ (1995) Extraction of mid-ocean-ridge basalt from the upwelling mantle by focused flow of melt in dunite channels. Nature 375:747–753

Kelemen PB, Hirth G, Shimizu N, Spiegelman M, Dick HJ (1997) A review of melt migration processes in the adiabatically upwelling mantle beneath oceanic spreading ridges. Philos Trans R Soc A Math Phys Eng Sci 355:238–318

Kerr RC, Tait SR (1985) Convective exchange between pore fluid and an overlying reservoir of denser fluid: a post-cumulus process in layered intrusions. Earth Planet Sci Lett 75:147–156

Kerr RC, Tait SR (1986) Crystallization and compositional convection in a porous medium with application to layered igneous intrusions. J Geophys Res 91:3591–3608

Klemme S, Blundy JD (2002) Experimental constraints on major and trace element partitioning during partial melting of eclogite. Geochim Cosmochim Acta 66:3109–3123

Kress VC, Carmichael IS (1991) The compressibility of silicate liquids containing Fe_2O_3 and the effect of composition, temperature, oxygen fugacity and pressure on their redox states. Contrib Mineral Petrol 108:82–92

Lange RA (1997) A revised model for the density and thermal expansivity of K_2O-Na_2O-CaO-MgO-Al_2O_3-SiO_2 liquids from 700 to 1900 K: extension to crustal magmatic temperatures. Contrib Mineral Petrol 130:1–11

Lange RA, Carmichael IS (1987) Densities of $Na2O$–$K2O$–CaO-MgO–FeO-$Fe2O3$–$Al2O3$–$TiO2$-$SiO2$ liquids: new measurements and derived partial molar properties. Geochim Cosmochim Acta 51:2931–2946

Lapwood ER (1948) Convection of a fluid in a porous medium. Proc Cambridge Phil Soc 44:508–521

Larsen RB, Brooks CK (1994) Origin and evolution of gabbroic pegmatites in the Skaergaard intrusion, East Greenland. J Petrol 35:1651–1679

Libourel G (1999) Systematics of calcium partitioning between olivine and silicate melt: implications for melt structure and calcium content of magmatic olivines. Contrib Mineral Petrol 136:63–80

Loncarevic BD, Feininger T, Lefevre D (1990) The Sept Iles layered mafic intrusion: geophysical expression. Can J Earth Sci 27:501–512

MacLeod CJ, Yaouancq G (2000) A fossil lens in the Oman ophiolite: implications for magma chamber processes at fast spreading ridges. Earth Planet Sci Lett 176:357–373

Marsh BD (1996) Solidification fronts and magmatic evolution. Mineral Mag 60:5–40

Martin D, Griffiths RW, Campbell IH (1987) Compositional and thermal convection in magma chambers. Contrib Mineral Petrol 96:465–475

Mathez EA, Hunter RH, Kinzler R (1997) Petrologic evolution of partially molten cumulate: the Atok section of the Bushveld Complex. Contrib Mineral Petrol 129:20–34

McKenzie DP (1984) The generation of compaction of partially molten rock. J Petrol 25:713–765

McKenzie DP (1985) The extraction of magma from the crust and mantle. Earth Planet Sci Lett 74:81–91

McKenzie DP (2011) Compaction and crystallization in magma chambers: towards a model for the Skaergaard intrusion. J Petrol 52:905–930

Meurer WP, Boudreau AE (1998a) Compaction of igneous cumulates. Part I: geochemical consequences for cumulates and liquid fractionation trends. J Geol 106:281–292

Meurer WP, Boudreau AE (1998b) Compaction of igneous cumulates. Part II: compaction and the development of igneous foliations. J Geol 106:293–304

Morgan Z, Liang Y (2003) An experimental and numerical study of the kinetics of harzburgite reactive dissolution with applications to dunite dyke formation. Earth Planet Sci Lett 214:59–74

Morse SA (1979) Kiglapait geochemistry. I: systematics, sampling, and density. J Petrol 20:555–590

Morse SA (1982) Adcumulus growth of anorthosite at the base of the lunar crust. J Geophys Res 87:10–18

Morse SA (1986) Convection in aid of adcumulus growth. J Petrol 27:1183–1214

Morse SA (1988) Motion of crystals, solute, and heat in layered intrusions. Can Mineral 26:209–224

Morse SA (1990) The differentiation of the Skaergaard intrusion. A discussion of Hunter and Sparks. Contrib Mineral Petrol 95:451–461

Morse SA (2008) Compositional convection trumps silicate liquid immiscibility in layered intrusions: a discussion of "Liquid immiscibility and the evolution of basaltic magmas" by Veksler et al. J Petrol 48:2187–2210

Morse SA (2011) The fractional latent heat of crystallizing magmas. Am Mineral 96:682–689

Namur O, Charlier B, Toplis MJ, Higgins MD, Liégeois JP, Vander Auwera J (2010) Crystallization sequence and magma chamber processes in the ferrobasaltic Sept Iles layered intrusion, Canada. J Petrol 51:1203–1236

Namur O, Charlier B, Toplis MJ, Higgins MD, Hounsell V, Liégeois JP, Vander Auwera J (2011a) Differentiation of tholeiitic basalt to A-type granite in the Sept Iles layered intrusion, Canada. J Petrol 52:487–539

Namur O, Charlier B, Pirard C, Hermann J, Liégeois JP, Vander Auwera J (2011b) Anorthosite formation by plagioclase flotation in ferrobasalt and implications for the lunar crust. Geochim Cosmochim Acta 75:4998–5018

Nield DA (1968) Onset of thermohaline convection in a porous medium. Wat Resour Res 4:553–560

Nielsen TF (2004) The shape and volume of the Skaergaard intrusion, Greenland: implications for mass balance and bulk composition. J Petrol 45:507–530

Ochs FA, Lange RA (1997) The partial molar volume, thermal expansivity, and compressibility of H_2O in $NaAlSi_3O_8$ liquid: new measurements and an internally consistent model. Contrib Mineral Petrol 129:155–165

Ochs FA, Lange RA (1999) The density of hydrous magmatic liquids. Science 283:1314–1317

Philpotts AR, Carroll M (1996) Physical properties of partly melted tholeiitic basalt. Geology 24:1029–1032

Philpotts AR, Carroll M, Hill JM (1996) Crystal-mush compaction and the origin of pegmatitic segregation sheets in a thick flood-basalt flow in the Mesozoic Hartford basin, Connecticut. J Petrol 37:811–836

Philpotts AR, Shi J, Brutsman C (1998) Role of plagioclase crystal chains in the differentiation of partly crystallized basaltic magma. Nature 395:343–346

Philpotts AR, Brustman CM, Shi J, Carlson WD, Denison C (1999) Plagioclase-chain networks in slowly cooled basaltic magma. Am Mineral 55:105–126

Pinkerton H, Norton GE (1995) Rheological properties of basaltic lavas at sub-liquidus temperatures: laboratory and field measurements on lavas from Mount Etna. J Volcanol Geotherm Res 68:307–323

Sato H (2005) Viscosity measurement of subliquidus magmas: 1707 basalt of Fuji Volcano. J Mineral Petrol Sci 100:133–142

Scott DR, Stevenson DJ (1986) Magma ascent by porous flow. J Geophys Res 91:9283–9296

Shirley ND (1986) Compaction of igneous cumulates. J Geol 94:795–809

Sparks RS, Huppert HE (1984) Density changes during the fractional crystallization of basaltic magmas: fluid dynamic implications. Contrib Mineral Petrol 85:300–309

Sparks RS, Huppert HE, Kerr RC, McKenzie DP, Tait SR (1985) Postcumulus processes in layered intrusions. Geol Mag 122:555–568

Tait SR, Jaupart C (1989) Compositional convection in viscous melts. Nature 338:571–574

Tait SR, Jaupart C (1992) Compositional convection in a reactive crystalline mush and melt differentiation. J Geophys Res 97:6735–6756

Tait SR, Huppert HE, Sparks RS (1984) The role of compositional convection in the formation of accumulate rocks. Lithos 17:139–146

Tait SR, Jahrling K, Jaupart C (1992) The planform of compositional convection and chimney formation in a mushy layer. Nature 359:406–408

Tegner C (1997) Iron in plagioclase as a monitor of the differentiation of the Skaergaard intrusion. Contrib Mineral Petrol 128:45–51

Tegner C, Thy P, Holness MB, Jakobsen JK, Lesher CE (2009) Differentiation and compaction in the Skaergaard intrusion. J Petrol 50:813–840

Thy P, Lesher CE, Nielsen TF, Brooks CK (2006) Experimental constraints on the Skaergaard liquid line of descent. Lithos 92:154–180

Thy P, Lesher CE, Tegner C (2009) The Skaergaard liquid line of descent revisited. Contrib Mineral Petrol 157:735–747

Toplis MJ, Carroll MR (1995) An experimental study of the influence of oxygen fugacity on Fe-Ti oxide stability, phase relations, and mineral-melt equilibria in ferro-basaltic systems. J Petrol 36:1137–1170

Toplis MJ, Carroll MR (1996) Differentiation of ferro-basaltic magmas under conditions open and closed to oxygen: implications for the Skaergaard intrusion and other natural systems. J Petrol 37:837–858

Toplis MJ, Dingwell DB, Libourel G (1994) The effect of phosphorous on the iron redox ratio, viscosity, and density of an evolved ferro-basalt. Contrib Mineral Petrol 117:293–304

Toplis MJ, Brown WL, Pupier E (2008) Plagioclase in the Skaergaard intrusion. Part 1: core and rim compositions in the Layered Series. Contrib Mineral Petrol 155:329–340

Van Den Bleeken G, Müntener O, Ulmer P (2010) Reaction processes between tholeiitic melt and residual peridotite in the uppermost mantle: an experimental study at 0.8 GPa. J Petrol 51:153–183

Vanderhaege O (2001) Melt segregation, pervasive melt migration and magma mobility in the continental crust: the structural record from pores to orogens. Phys Chem Earth 26:213–223

Wager LR, Brown GM (1968) Layered igneous rocks. Oliver and Boyd, London

Wark DA, Watson EB (2000) Effect of grain size on the distribution and transport of deep-seated fluid and melts. Geophys Res Lett 27:2029–2032

Worster MG (1992) Instabilities of the liquid and mushy regions during solidification of alloys. J Fluid Mech 237:649–669